

**A Study on Dynamic and Static Recrystallization
Behaviors and Microstructure Evolution Prediction of
Die Steels**

2001 2

2000 12 19

Abstract	
.....	
List of Table and Photographs	
List of Figures	
1.	1
1.1	1
1.2	2
1.3	3
2.	4
2.1 가	4
2.1.1	4
2.1.2	6
2.1.3	7
2.2	8
3.	12
3.1	12
3.1.1	12
3.1.2	13
3.1.3	14
3.2	15

3.3	15
4.	18
4.1	18
4.1.1	18
4.1.2	23
4.1.3	27
4.2	29
4.2.1	29
4.2.2	36
4.2.3	41
4.3	55
5.	66
	68

A Study on Dynamic and Static Recrystallization Behaviors and Microstructure Evolution Prediction of Die Steels

Ho-Seung Jeong

Department of Mechanical Engineering Graduate School,
Korea Maritime University

ABSTRACT

Evaluation of microstructural changes during open die forging of heavy ingots is important for process control. The objective of the control of forging parameters, such as shape of the dies, reduction, temperature and sequence of passes, is to maximize the forging effects and to minimize inhomogeneities of mechanical properties.

A numerical analysis was performed to predict flow curves and dynamic and static recrystallization behaviors of die steel(0.36%C, 1.1%Mn and 1.21%Cr) from hot compression test results. The hot compression tests were carried out in the ranges of temperature 950 ~ 1150 °C and strain rate 0.01 ~ 1.0sec⁻¹. The modeling equation for flow curves was a function of strain, strain rate and temperature. Models for predicting the evolution of microstructure in die steel during thermomechanical processing was developed in terms of dynamic, static recrystallization and grain growth phenomena. The microstructure model was

combined with rigid visco-plastic finite element modeling to predict microstructure development. Predicted microstructure is consistent with results obtained in multiple compression tests.

For the grain growth evolution, hot compression test carried out the temperature of 950 and 1150 °C, and the strain rate of 0.01 and 1.0sec⁻¹. The specimens were compressed 10%, 20% and 30% in height, unloaded and held for holding times at isothermal condition resulting in static and metadynamic recrystallization in specimens.

The softening occurred during the holding time between the first and the second compression was calculated from the experimental result. Predicted grain size and load are consistent with experiment results from double compression test with constant velocity. Therefore, the usefulness of the program is verified.

σ_p	:	(peak stress)
σ_e	:	가
σ_s	:	(steady state stress)
$\bar{\sigma}$:	(effective stress)
σ_{ij}'	:	(deviatoric stress tensor)
ϵ_p	:	
ϵ_c	:	
$\bar{\epsilon}$:	(effective strain)
$\dot{\bar{\epsilon}}$:	(effective strain rate)
$\dot{\epsilon}_{ij}$:	(strain rate tensor)
$\Delta\sigma$:	
Δt	:	
Z	:	Zener-Hollomon Parameter
X_{dyn}	:	(dynamic recrystallization volume fraction)
X	:	(static recrystallization volume fraction)
K	:	(penalty function)
\bar{D}	:	(mean grain size)
d_{rex}	:	(recrystallized grain size)
D_o	:	(initial grain size)
Q	:	(activation energy)
n	:	(strain rate sensitivity)

List of Table and Photographs

Table

Table 1 Chemical composition of die steel

Photographs

Photo 1 Microstructure of 50% compressed specimen at 950 and $\dot{\epsilon}=0.01/s$

Photo 2 Microstructure of 50% compressed specimen at 1050 and $\dot{\epsilon}=0.1/s$

Photo 3 Microstructure of 50% compressed specimen at 1150 and $\dot{\epsilon}=0.1/s$

Photo 4 Microstructure of 50% compressed specimen at 950 and $\dot{\epsilon}=1.0/s$

Photo 5 Microstructure of 50% compressed specimen at 1050 and $\dot{\epsilon}=1.0/s$

Photo 6 Microstructure of 50% compressed specimen at 1150 and $\dot{\epsilon}=1.0/s$

Photo 7 Microstructure of 50% compressed casting specimen at 1050 and $\dot{\epsilon}=1.0/s$

Photo 8 Microstructure of 50% compressed casting specimen at 1150 and $\dot{\epsilon}=1.0/s$

Photo 9 Microstructure of 20% compressed specimen at 950 , $\dot{\epsilon}=1.0/s$ and 5sec holding

Photo 10 Microstructure of 20% compressed specimen at 950 , $\dot{\epsilon}=1.0/s$ and 10sec holding

Photo 11 Microstructure of 20% compressed specimen at 950 , $\dot{\epsilon}=1.0/s$ and 100sec holding

Photo 12 Microstructure of 20% compressed specimen at 950 , $\dot{\epsilon}=1.0/s$ and 600sec holding

Photo 13 Microstructure of 20% compressed specimen at 1150 , $\dot{\epsilon}=1.0/s$ and 5sec holding

Photo 14 Microstructure of 20% compressed specimen at 1150 , $\dot{\varepsilon}=1.0/\text{s}$ and 20sec holding

Photo 15 Microstructure of 20% compressed specimen at 1150 , $\dot{\varepsilon}=1.0/\text{s}$ and 100sec holding

Photo 16 Microstructure of 20% compressed specimen at 1150 , $\dot{\varepsilon}=1.0/\text{s}$ and 600sec holding

Photo 17 Microstructure of second compression at $v=1\text{mm/s}$, 1150 and 100s holding

Photo 18 Microstructure of second compression at $v=1\text{mm/s}$, 1150 and 600s holding

List of Figures

- Fig. 1 Course of recrystallization
- Fig. 2 Flow stress curves in hot forming
- Fig. 3 Testing equipment
- Fig. 4 Experimental method of single compression
- Fig. 5 Experimental method of double compression
- Fig. 6 Initial finite element mesh for the simulation
- Fig. 7 Flow chart for microstructure simulation
- Fig. 8 Stress vs Strain rate at various temperature by hyperbolic law
- Fig. 9 Strain dependence of strain rate sensibility(n)
- Fig. 10 $\sinh(\quad)$ vs temperature at various strain rate
- Fig. 11 Strain dependence of activation energy(Q)
- Fig. 12 Dependence of $\sinh(\quad)$ on Zener-Hollomon parameter
- Fig. 13 Schematic view of the effect on dynamic softening
- Fig. 14 Experimental and predicted flow curves at $\dot{\epsilon}=0.01/s$
- Fig. 15 Experimental and predicted flow curves at $\dot{\epsilon}=0.1/s$
- Fig. 16 Experimental and predicted flow curves at $\dot{\epsilon}=1.0/s$
- Fig. 17 Experimental and predicted grain growth curves at 950 °C and 1150 °C
- Fig. 18 Comparison of flow curves at $\dot{\epsilon}=0.01/s$
- Fig. 19 Comparison of flow curves at $\dot{\epsilon}=0.1/s$
- Fig. 20 Comparison of flow curves at $\dot{\epsilon}=1.0/s$
- Fig. 21 Flow curves obtained from interrupted compression test at $\dot{\epsilon}=0.01/s$,
950 °C and (a) 10% compression (b) 20% compression
- Fig. 22 Flow curves obtained from interrupted compression test at $\dot{\epsilon}=0.1/s$,
950 °C and (a) 10% compression (b) 20% compression
- Fig. 23 Flow curves obtained from interrupted compression test at $\dot{\epsilon}=0.01/s$,

1150 and (a) 10% compression (b) 20% compression

Fig. 24 Flow curves obtained from interrupted compression test at $\dot{\epsilon}=0.1/s$,

1150 and (a) 10% compression (b) 20% compression

Fig. 25 Flow curves obtained from interrupted compression test at $v=1\text{mm/s}$

and (a) 950 (b) 1150

Fig. 26 Strain effect on the rate of softening at 950 and (a) $\dot{\epsilon}=0.01/s$

(b) $\dot{\epsilon}=0.1/s$

Fig. 27 Strain effect on the rate of softening at 1150 and (a) $\dot{\epsilon}=0.01/s$

(b) $\dot{\epsilon}=0.1/s$

Fig. 28 Strain rate effect on the rate of softening at (a) 950 (b) 1150

Fig. 29 Temperature effect on the rate of softening at (a) $\dot{\epsilon}=0.01/s$ (b) $\dot{\epsilon}=0.1/s$

Fig. 30 Diagram for each microstructure photographic point

Fig. 31 Mean grain size from simulation result at $v=1\text{mm/s}$, 1150 and

(a) 100sec holding (b) 600sec holding

Fig. 32 Comparison of grain size between experimental and predicted results at

$v=1\text{mm/s}$, 1150 and (a) axial direction (b) radial direction

Fig. 33 Distribution of mean grain size after 16.7% second compression at

$v=1\text{mm/s}$ and 1150

Fig. 34 Distribution of mean grain size after 100sec holding at $v=1\text{mm/s}$,

1150 and 16.7% compression

Fig. 35 Distribution of mean grain size after 600sec holding at $v=1\text{mm/s}$,

1150 and 16.7% compression

Fig. 36 Distribution of mean grain size after 36.7% second compression at

$v=1\text{mm/s}$, 1150 and 100sec holding

Fig. 37 Distribution of mean grain size after 36.7% second compression at

$v=1\text{mm/s}$, 1150 and 600sec holding

Fig. 38 Comparison of experimental and predicted load at $v=1\text{mm/s}$, 1150 and

600sec holding

1.

1.1

가

가

가

가

.

.

(casting)

(ingot)

(open die forging)

.

,

(die)

, , ,

가

.

가

(T),

($\dot{\epsilon}$),

(ϵ),

(σ),

(structure)

.

가

가

가

가

.

가

,

.

,

.

, (upsetting)

가 .

1.2

(static recrystallization, SRX), (dynamic recrystallization, DRX), (grain growth) [1- 15],

, , , , [16- 20].

Sellars [1]

, [2- 4]. Hernandez [5],

[6- 8]. Martine[9], Zhao [12]

HY- 100

. Cho [13] Al 6061

, Sun [15] (static) (metadynamic)

, , , Dandre [16]

Incornel 718

,

. Cho [17]

, Kwak

[18]

,

. Hwang Cho [20]

Al- 5wt% Mg

, Han

[21] SCM 440

C-Mn

[2- 11,17- 18,21]

2

1.3

가 , 가 , , , , 가 , (0.36% C, 1.1% Mn, 1.21% Cr) (0.01 1.0/ s), (950 1150), (10 50%), (5 600s) , , , , , , , , , (fractional softening) .

가 Fig. 1 (2) 가
(3) (4) 가

(ε_c :)
[1]. 가

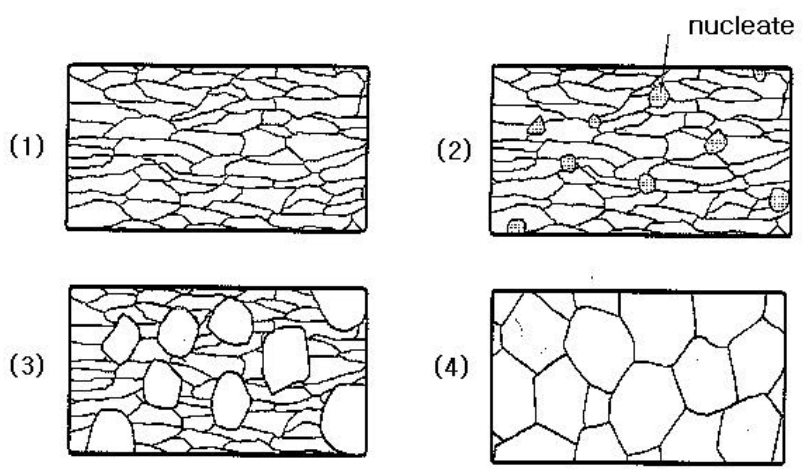


Fig. 1 Course of recrystallization

Fig. 2

(1) 가
가 , (2) (3)
가 (2)
가 (3)
가 가

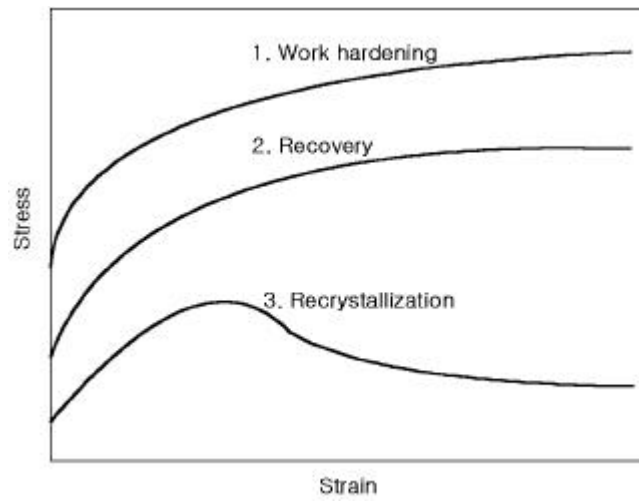


Fig. 2 Flow stress curves in hot forming

가 , ,

(ϵ_c ,)

2.1.2

가

가

가 .

,

, 가

.

,

가

.

2.1.3

가 가 (stress)

,

.

가

가

가

가 (grain growth)

,

가

.

가

.

2.2

(finite element)
(variational
principle), 가 (method of weighted residual), (energy
balance approach)

(elastic-plastic analysis),
(rigid-plastic analysis), 가
(viscoplastic analysis)

가

가

가

가

- (1) , .
- (2) .
- (3) .
- (4) Von Mises .
- (5) , .

V T_i 가 S_f v 가 S_v
 . 가
 (infinitesimal deformation)

() (equilibrium equation)

$$\sigma_{ij,i} = 0 \quad (2.1)$$

() (compatibility equation)

$$\dot{\epsilon}_{ij} = \frac{1}{2} (v_{i,j} + v_{j,i}) \quad (2.2)$$

$$\dot{\epsilon}_{i,i} = \dot{\epsilon}_v = 0 \quad (2.3)$$

() (constitutive equation)

$$\sigma_{ij}' = \frac{2}{3} \frac{\bar{\sigma}}{\bar{\epsilon}} \dot{\epsilon}_{ij} \quad (2.4)$$

$$\bar{\sigma} = \sqrt{\frac{3}{2} \sigma_{ij}' \sigma_{ij}'} \quad (2.5)$$

$$\bar{\epsilon} = \sqrt{\frac{2}{3} \dot{\epsilon}_{ij} \dot{\epsilon}_{ij}} \quad (2.6)$$

$$\sigma_{ij}', \quad \bar{\sigma}, \quad \bar{\epsilon}$$

() (boundary condition)

$$\sigma_{ij} n_j = T_i \quad \text{on } S_f \quad (2.7)$$

$$v_i = U_i \quad \text{on } S_v \quad (2.8)$$

$$n_j$$

(2.1)

$$\int_V \sigma_{ij,i} \delta v_i dV = 0 \quad (2.9)$$

$$(2.2) \quad (2.7) \quad \text{가}$$

$$\int_v \sigma_{ij} \delta \dot{\varepsilon}_{ij} dV - \int_{S_F} T_i \delta v_i dS = 0 \quad (2.10)$$

$$\sigma_{ij} = \sigma_{ij}' + \delta_{ij} \sigma_m \quad (2.11)$$

$$(2.10) \quad (2.11)$$

$$\int_v \sigma_{ij}' \delta \dot{\varepsilon}_{ij} dV + \int_v \sigma_m \delta \dot{\varepsilon}_v dV - \int_{S_F} T_i \delta v_i dS = 0 \quad (2.12)$$

가

$$(2.4) \quad (2.6)$$

$$\sigma_{ij}' \delta \dot{\varepsilon}_{ij} = \overline{\sigma} \delta \dot{\varepsilon}_{ij} \quad (2.13)$$

$$, \quad K = \frac{\sigma_m}{\dot{\varepsilon}_v} \quad (2.13) \quad K \quad (2.12)$$

$$\delta \pi = \int_v \overline{\sigma} \delta \dot{\varepsilon} dV + K \int_v \dot{\varepsilon}_v \delta \dot{\varepsilon}_v dV - \int_{S_F} T_i \delta v_i dS = 0 \quad (2.14)$$

K

$$(2.14)$$

$$f = - \frac{2}{\pi} m k \tan^{-1} \frac{|v_s|}{u_o} t \quad (2.15)$$

$$m, k, u_o, |v_s|$$

$$, v_s, t, v_s$$

$$t = -\frac{1}{v_s} [u\mathbf{i} + (v + v_D)\mathbf{j}] \tag{2.16}$$

$$v_s = \sqrt{u^2 + (v + v_D)^2} \tag{2.17}$$

3.

3.1

3.1.1

Fig. 3

Table 1. Chemical composition of die steel(wt.%)

Element	C	Si	Mn	P	S	Ni	Cr	Mo	V
Composition	0.36	0.26	1.10	0.006	0.003	0.07	1.21	0.26	0.027

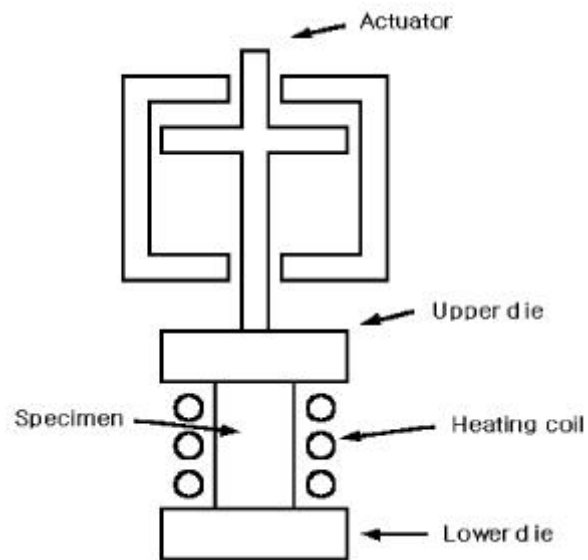


Fig. 3 Testing equipment

가 Fig. 4
 5 /sec 3
 0.01/s, 0.1/s, 1.0/s 950 , 1050 , 1150
 35%, 50% 가

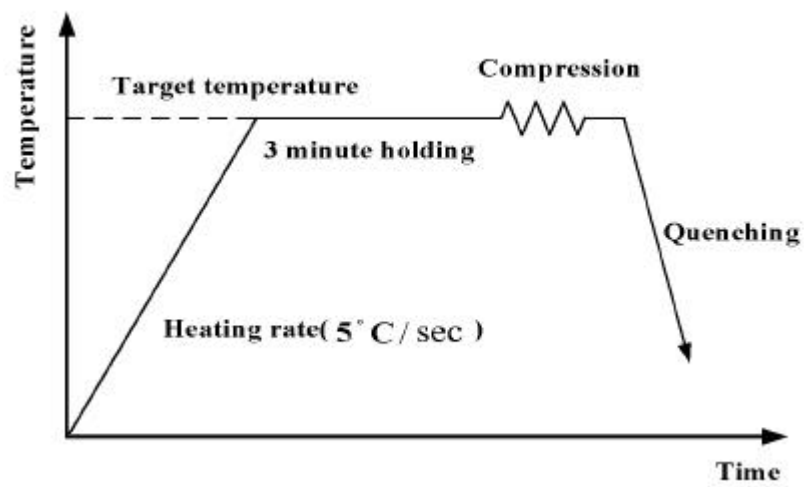


Fig. 4 Experimental method of single compression

(200ml), (20mg) (20ml)

3.1.2

,
 , 0.01/s,
 1.0/s 950 , 1150 10%, 20%, 30%
 , ,

0.01/s
 5sec, 10sec, 100sec, 600sec 1.0/s 5sec, 20sec, 100sec,
 600sec 가 .

3.1.3

,
 . Fig. 5 0.01/s, 0.1/s 950 , 1150
 10%, 20%
 , 0.01/s
 5sec, 10sec, 100sec, 600sec 0.1/s 5sec, 20sec, 100sec,
 600sec 50% 가

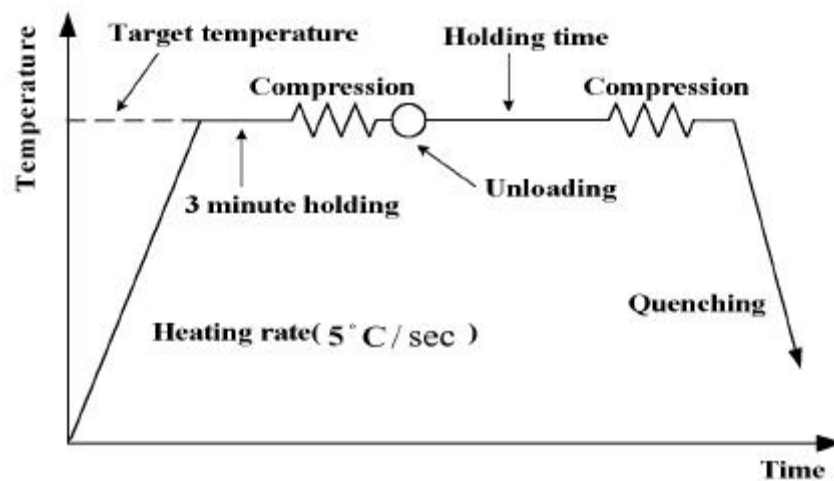


Fig. 5 Experimental method of double compressions

$$FS = \frac{\sigma_m - \sigma_{y2}}{\sigma_m - \sigma_{y1}} \tag{3.1}$$

， σ_m σ_{y1} σ_{y2}

3.2

Fig.5 950 ， 1150
1mm/s 16.7%
100sec, 600sec 20%

3.3

， Fig. 6
(element) 238
3.2

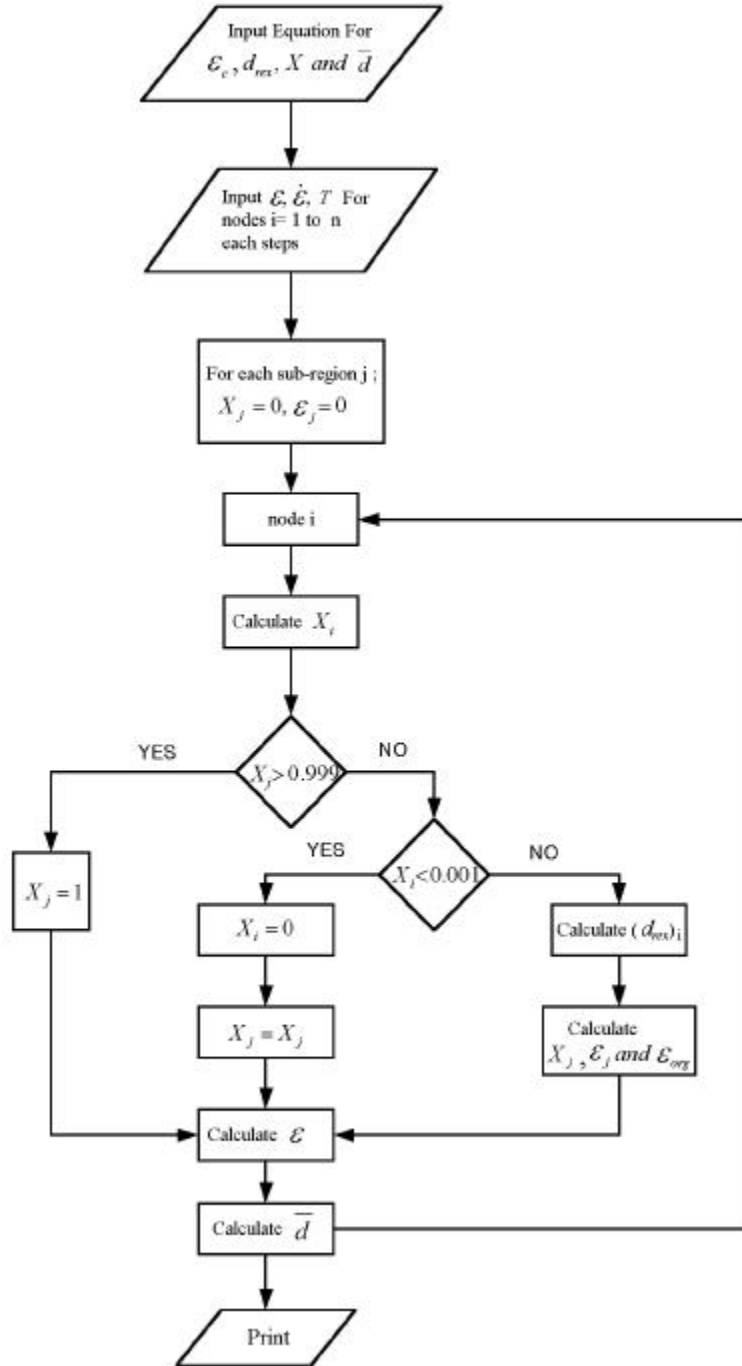


Fig. 7 Flow chart for microstructure simulation

4.

4.1

4.1.1

(), (T), ($\dot{\epsilon}$), (Q)
 , Zener - Hollomon
 Arrhenius
 - Zener - Hollomon
 [5].

$$\sigma = f(Z, \epsilon) \quad (4.1)$$

$$Z = \dot{\epsilon} \cdot \exp\left(\frac{Q}{RT}\right) \quad \text{Zener - Hollomon} \quad [5], Q$$

 (activation energy, $Jmol^{-1}$) , T
 (K), R 가 (gas constant, $8.314 Jmol^{-1}K^{-1}$) .
 , , , Arrhenius
 3가 가 .
 3가

$$\dot{\epsilon} = A' \exp(n'\sigma) \cdot \exp\left(-\frac{Q}{RT}\right) \quad (\text{exponential law}) \quad (4.2)$$

$$\dot{\epsilon} = A'' \sigma^{n''} \cdot \exp\left(-\frac{Q}{RT}\right) \quad (\text{power law}) \quad (4.3)$$

$$\dot{\epsilon} = A [\sinh(\alpha\sigma)]^n \cdot \exp\left(-\frac{Q}{RT}\right) \quad (\text{hyperbolic law}) \quad (4.4)$$

, A, A', A'', , n, n', n'' .

Arrhenius (4.2) n'

가

$$\dot{\epsilon} = \frac{1}{n} \left(\frac{Z}{A} \right)^{1/n} \quad (4.3)$$

가

n

.

$$\dot{\epsilon} = \frac{1}{n} \left(\frac{Z}{A} \right)^{1/n} \quad (4.4)$$

$$(4.2), (4.3)$$

Z 가

[4].

Z

Sellars

Tegart[5]

, Zener

- Hollomon

$$\dot{\epsilon} = \frac{1}{n} \left(\frac{Z}{A} \right)^{1/n} \quad (4.4)$$

$$Z = \dot{\epsilon} \cdot \exp \left(-\frac{Q}{RT} \right) = A [\sinh(\alpha \sigma)]^n \quad (4.5)$$

n

.

,

.

,

0.012

(MPa⁻¹)

[6].

0.01/s, 0.1/s, 1.0/s,

950 , 1050 , 1150

=0.012(MPa⁻¹)

$$\dot{\epsilon} = \frac{1}{n} \left(\frac{Z}{A} \right)^{1/n} \quad (4.6)$$

n

.

$$\ln \dot{\epsilon} = n \ln [\sinh(\alpha \sigma)] + C \quad (4.6)$$

$$\dot{\epsilon} = \frac{1}{n} \left(\frac{Z}{A} \right)^{1/n} \quad (4.6)$$

Fig. 8

n

,

가

. Fig. 9

n

n=4.046

.

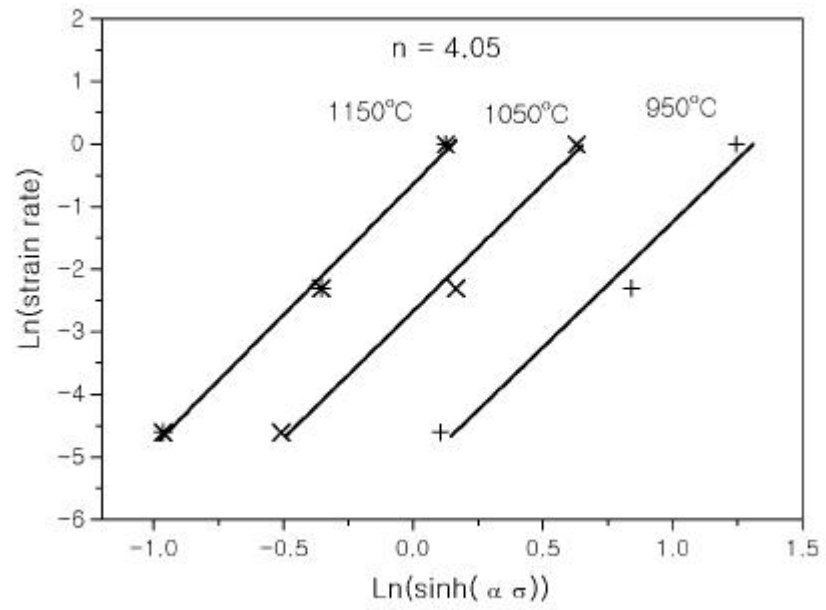


Fig. 8 Stress vs Strain rate at various temperature by hyperbolic law

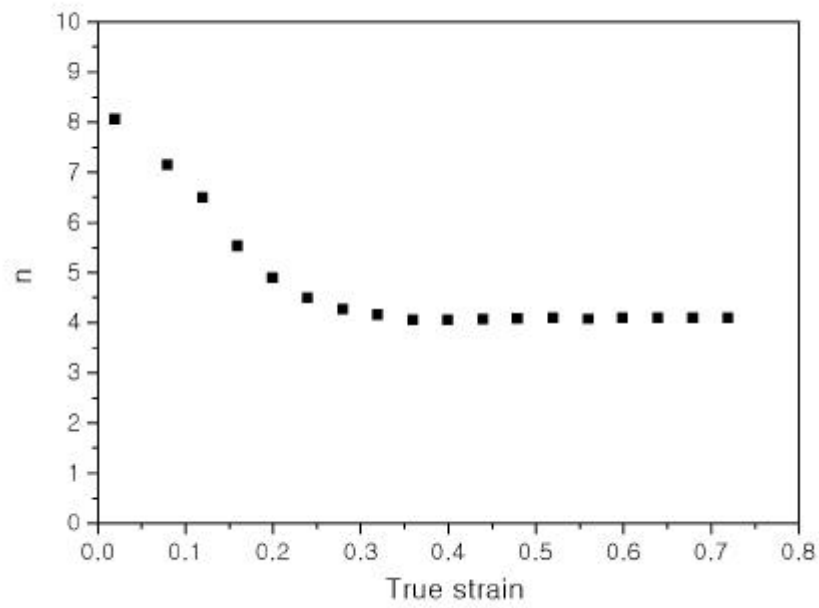


Fig. 9 Strain dependence of strain rate sensibility(n)

가

$$\ln [\sinh (\alpha \sigma)] = \frac{1}{T} \quad .$$

$$(4.5) \quad \ln \ln A + n \ln [\sinh (\alpha \sigma)] = \ln \dot{\epsilon} + \frac{Q}{RT} \quad \text{가} \quad \ln [\sinh (\alpha \sigma)] =$$

$$\frac{Q}{nRT} + \left(\frac{\ln \dot{\epsilon} - \ln A}{n} \right) \quad \text{가} \quad \ln [\sinh (\alpha \sigma)] = \frac{Q}{nRT} + C(\quad)$$

, n, R

Q . Fig. 10

, n, R

n, R . Fig. 11

.

가 , Q=330(kJ/mole) . C-Mn

Sellars [1] 312(kJ/mole) .

C-Mn 가 .

(4.5) , n, Q Fig. 12 ,

, , n=4.041

n=4.046 . 가

(4.7) .

$$\dot{\epsilon} = 6.956 \times 10^{11} [\sinh (0.012 \sigma)]^{4.046} \exp \left(- \frac{Q}{RT} \right) \quad (0.01 \leq \dot{\epsilon} \leq 1.0) \quad (4.7)$$

, , ,

.

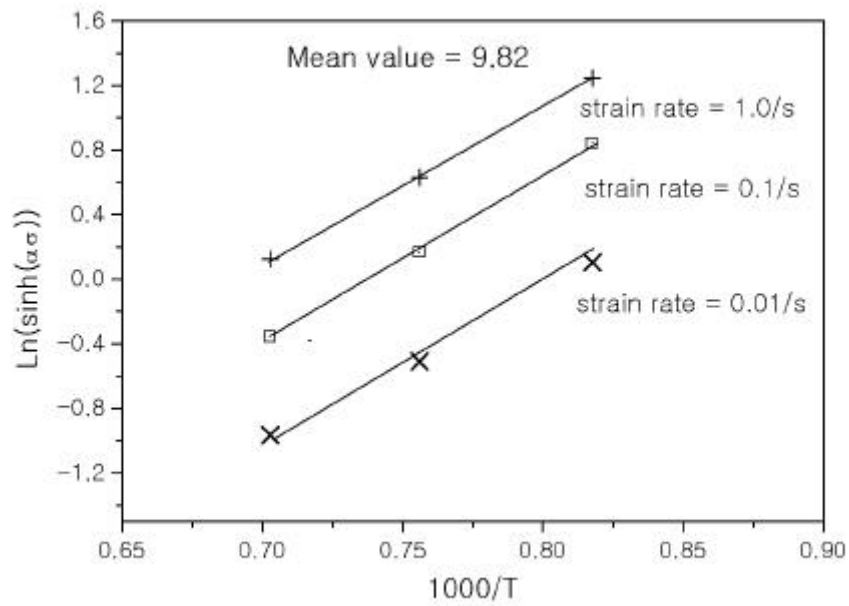


Fig. 10 $\sinh(\quad)$ vs temperature at various strain rate

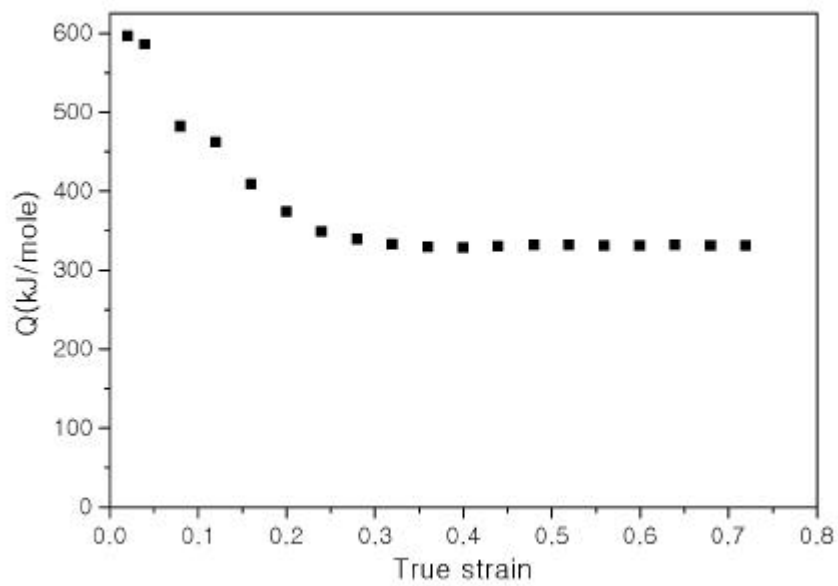


Fig. 11 Strain dependence of activation energy (Q)

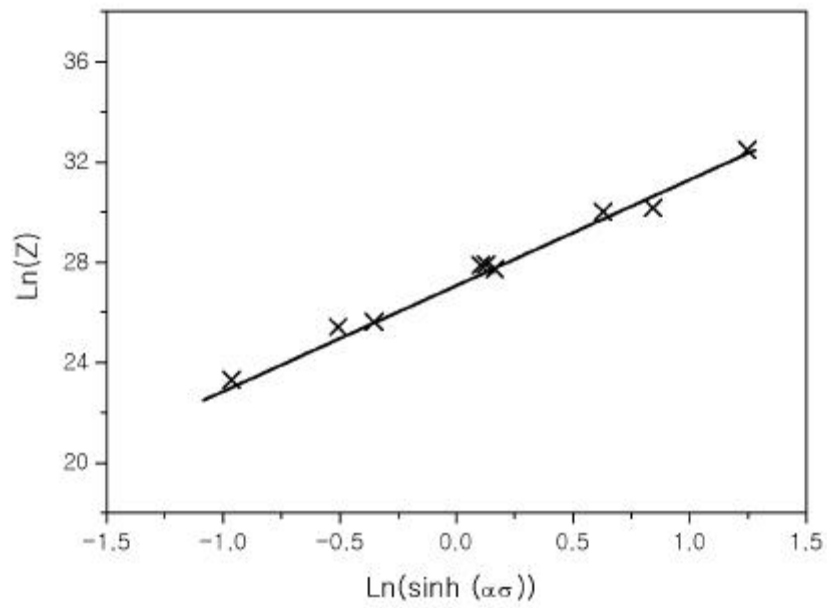


Fig. 12 Dependence of $\sinh(\quad)$ on Zener-Hollomon parameter

4.1.2

가 가 ,
[6].

$$\sigma = \sigma_e - \Delta\sigma \quad (4.8)$$

$$\sigma_e = \sigma_p [1 - \exp(-C\varepsilon)]^m \quad (\varepsilon < \varepsilon_p) \quad (4.9)$$

$$\Delta\sigma = (\sigma_p - \sigma_s) [1 - \exp(-k(\frac{\varepsilon - \alpha\varepsilon_p}{\varepsilon_p})^{m'})] \quad (\varepsilon > \alpha\varepsilon_p) \quad (4.10)$$

Fig. 13 σ_e 가 , $\Delta\sigma$
가 .

$$, \quad (4.11) \quad [6].$$

$$\sigma = \sigma_p [1 - \exp(-C\varepsilon)]^m - (\sigma_p - \sigma_s) [1 - \exp(-k(\frac{\varepsilon - \alpha\varepsilon_p}{\varepsilon_p})^{m'})] \quad (4.11)$$

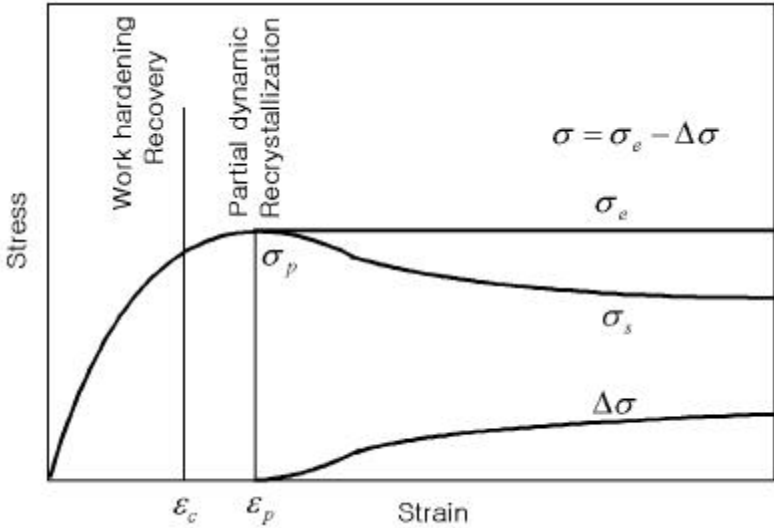


Fig. 13 Schematic view of the effect on dynamic softening

($\alpha \epsilon_p$)

[6] α [6],

[7] 0.95, [8], [21] 5/6, [2] 0.8 .

c, m, k, m ' ,

, , , ,

Z/A .

$$C = 15.83 \cdot \epsilon^{-0.2248} \exp\left(-\frac{0.0277 Q}{R T}\right) \quad (4.12)$$

$$m = 0.478 \cdot \epsilon^{-0.0449} \exp\left(\frac{-0.00871Q}{RT}\right) \quad (4.13)$$

$$k = 0.93 + 0.136 \left(\frac{Z}{A} \right) \quad (4.14)$$

$$m' = 0.202 \dot{\epsilon}^{0.174} \exp\left(-\frac{0.0955Q}{RT}\right) \quad (4.15)$$

$$\epsilon_p = 0.07 \dot{\epsilon}^{0.176} \exp\left(-\frac{0.0513Q}{RT}\right) \quad (4.16)$$

$$\epsilon_c = 0.8 \epsilon_p$$

$$\sigma_p = 0.66 \dot{\epsilon}^{0.367} \exp(-5.618\epsilon_p) \exp\left(\frac{0.234Q}{RT}\right) \quad (4.17)$$

$$\sigma_s = 67.3 + 13.35 \ln\left(\frac{Z}{A}\right) + 0.92\left(\ln\left(\frac{Z}{A}\right)\right)^2 \quad (4.18)$$

$$(4.12) \quad (4.18) \quad (4.11)$$

Fig. 14 16 ,

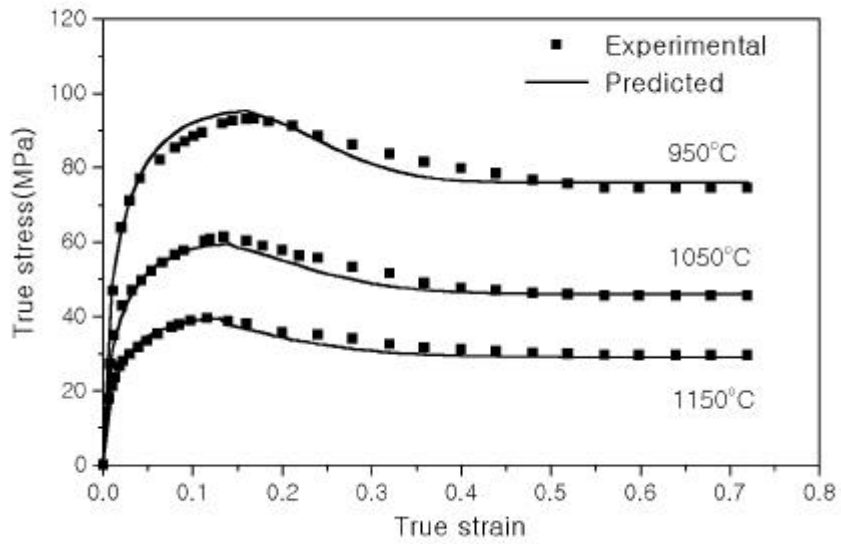


Fig. 14 Experimental and predicted flow curves $\dot{\epsilon}=0.01/s$

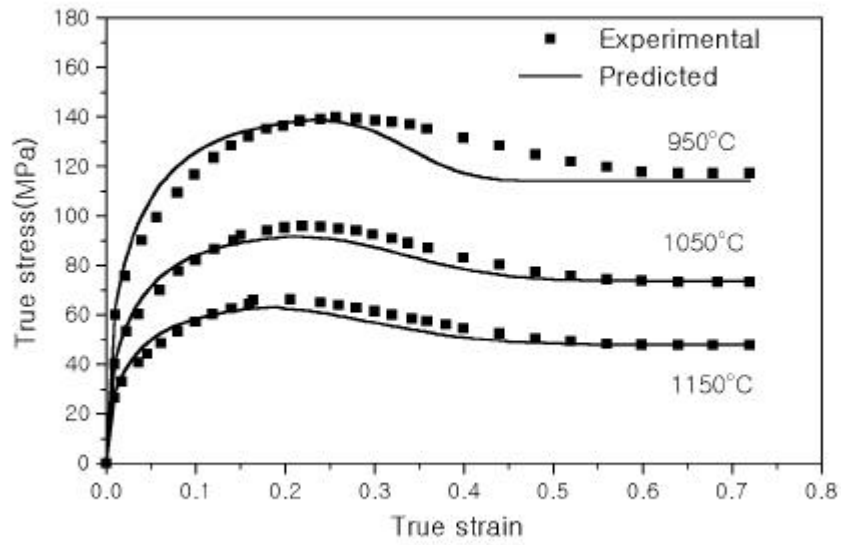


Fig. 15 Experimental and predicted flow curves for $\dot{\epsilon}=0.1/s$

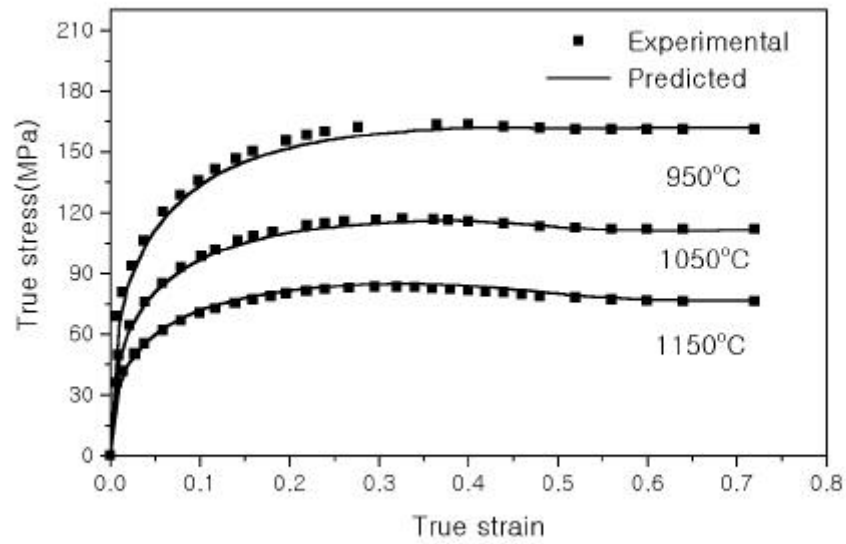


Fig. 16 Experimental and predicted flow curves for $\dot{\epsilon}=1.0/s$

4.1.3

$$X_{dyn} = \left[1 - \exp \left(-k \left(\frac{\varepsilon - \varepsilon_c}{\varepsilon_c} \right)^{m'} \right) \right] \quad (4.10)$$

$$k = 0.654 + 0.146 \ln \left(\frac{Z}{A} \right) \quad (4.20)$$

$$m' = 1.4737 - 0.1107 \ln \left(\frac{Z}{A} \right) \quad (4.21)$$

$$d_{rex} = 1.2 \cdot 10^4 Z^{-0.21} \quad (4.22)$$

$$\overline{D} = \sqrt{\frac{D_o^2 d_{dyn}^2}{D_o^2 X_{dyn}^2 + d_{dyn}^2 (1 - X_{dyn})^2}} \quad (4.23)$$

Sellars [2] C-Mn

$$X = 1 - \exp \left[- \ln 2 \cdot \left(\frac{t}{t_{0.5}} \right)^2 \right] \quad (4.24)$$

$$t_{0.5} = 2.5 \cdot 10^{-19} d_{ini}^2 \varepsilon^{-4} \exp \left(- \frac{300000}{R T} \right) \quad \varepsilon \leq 0.8 \varepsilon_p \quad (4.25)$$

$$t_{0.5} = 1.06 \cdot 10^{-5} Z^{-0.6} \exp \left(- \frac{300000}{R T} \right) \quad \varepsilon \geq 0.8 \varepsilon_p \quad (4.26)$$

X , $t_{0.5}$ 50%

$$d_{rex} = 0.5 d_{ini}^{0.67} \varepsilon^{-1} (\mu m), \quad (\varepsilon \leq \varepsilon^*) \quad (4.27)$$

$$d_{rex} = 1.8 \cdot 10^3 Z^{-0.15} (\mu m), \quad (\varepsilon \geq \varepsilon^*) \quad (4.28)$$

$$, \quad \varepsilon^* = 0.57 d_{ini}^{0.17} \varepsilon_p .$$

$$d^{10} = d_{rex}^{10} + 5.02 \cdot 10^{53} t \exp \left(- \frac{914000}{R T} \right), \quad T \leq 1273 (K) \quad (4.29)$$

$$d^{10} = d_{rex}^{10} + 3.87 \cdot 10^{32} t \exp \left(- \frac{400000}{R T} \right), \quad T \geq 1273 (K) \quad (4.30)$$

d_{rex} , d .

Sellars

,

,

[13].

3.1.2

(4.31) . Fig. 17

$$\overline{D}^3 = D_o^3 + 1.8 \cdot 10^{16} t \exp\left(-\frac{Q}{R T}\right) \quad (4.31)$$

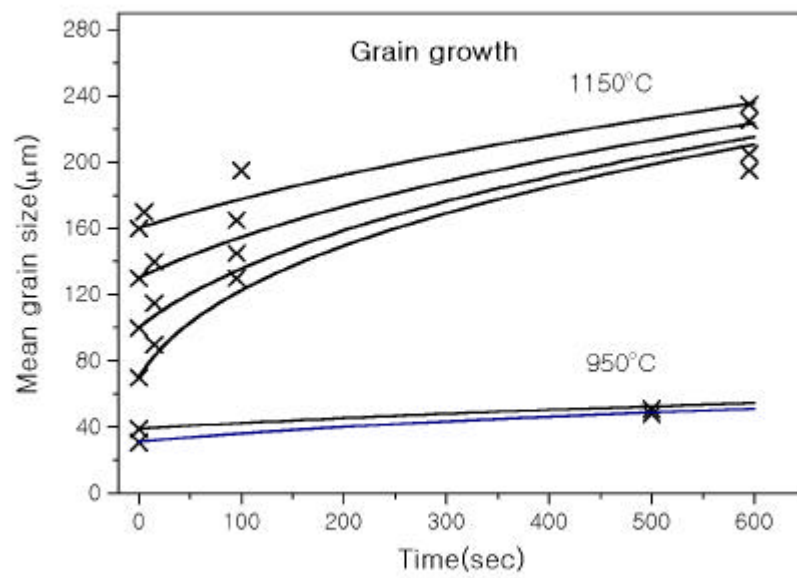


Fig. 17 Experimental and predicted grain growth curves at 950 and 1150

4.2

4.2.1

(Photo 1 6). Photo 1

950 , 가 0.01/s 가
 Photo 4 가 가
 . Photo 3 Photo 6 1150 가 0.1/s
 1.0/s 가 Photo 6
 가 . Photo 4 6
 가 . 가 가
 , (4.22)
 가
 . 가 , Photo
 4 950 , 50% 가 1.0/s ,
 가 가
 가 ,

가 가

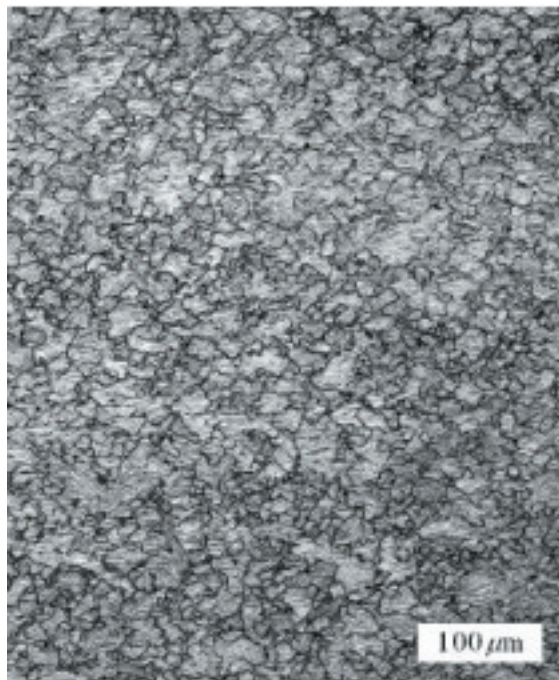


Photo 1 Microstructure of 50% compressed specimen at 950 and $\dot{\epsilon}=0.01/s$



Photo 2 Microstructure of 50% compressed specimen at 1050 °C and $\dot{\epsilon}=0.1/s$

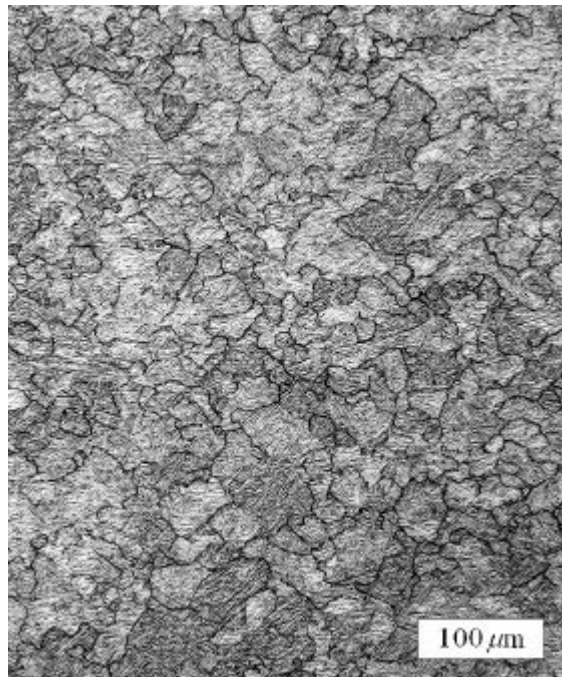


Photo 3 Microstructure of 50% compressed specimen at 1150 °C and $\dot{\epsilon}=0.1/s$

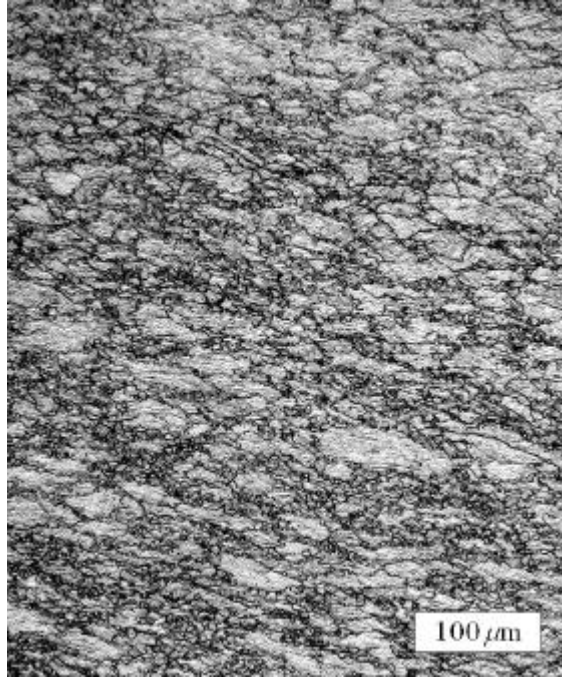


Photo 4 Microstructure of 50% compressed specimen at 950 °C and $\dot{\epsilon}=1.0/\text{s}$

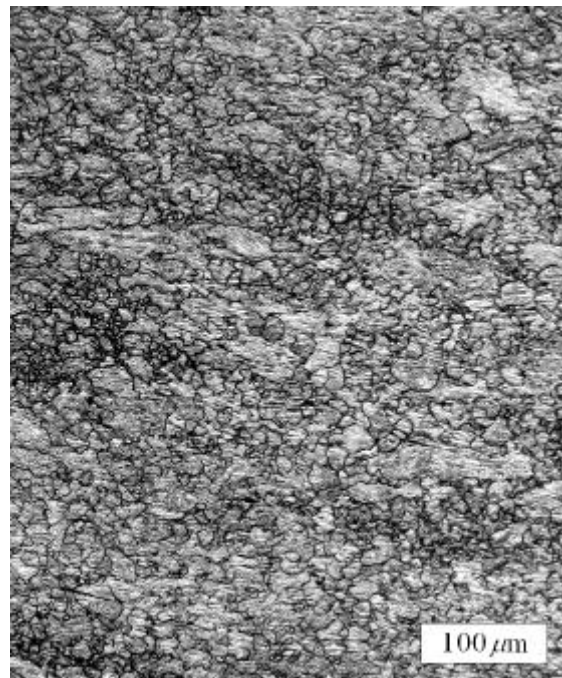


Photo 5 Microstructure of 50% compressed specimen at 1050 °C and $\dot{\epsilon}=1.0/\text{s}$

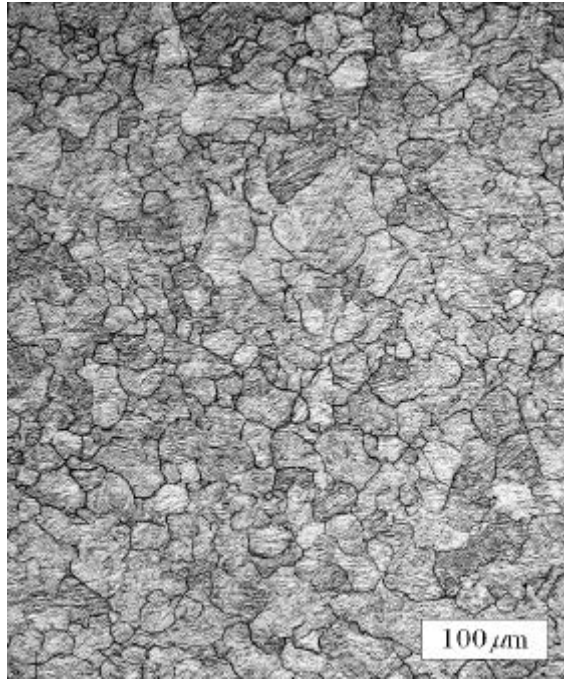


Photo 6 Microstructure of 50% compressed specimen at 1150 °C and $\dot{\epsilon}=1.0/\text{s}$

. Fig. 18 20

,

6.5%

.

가

.

가 0.1s^{-1}

가

0.1s^{-1}

가

가

. Photo 7 8

Photo 1 6

,

.

.

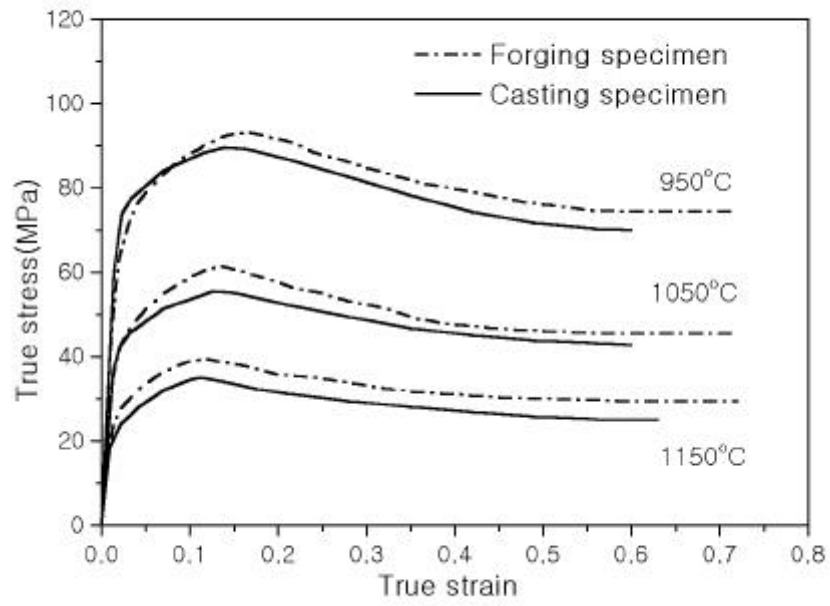


Fig. 18 Comparison of flow curves at $\dot{\epsilon}=0.01/s$

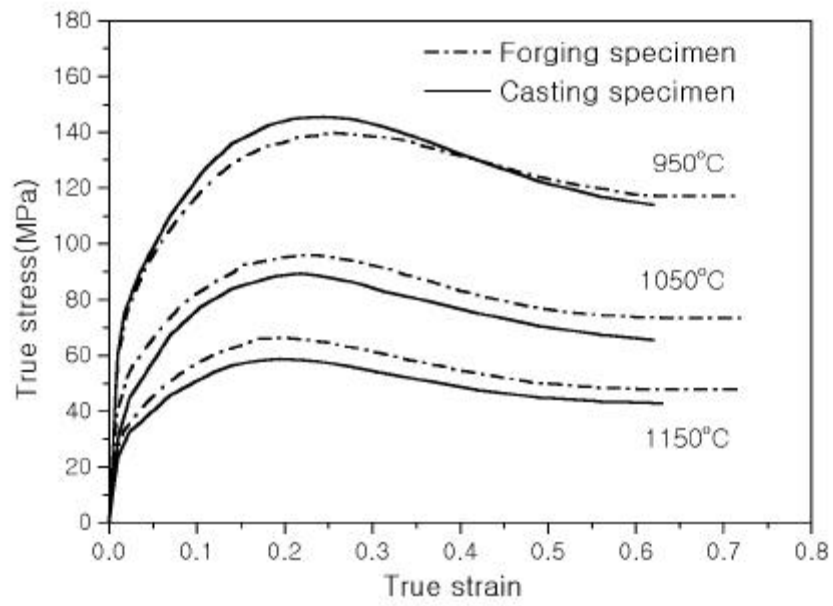


Fig. 19 Comparison of flow curves at $\dot{\epsilon}=0.1/s$

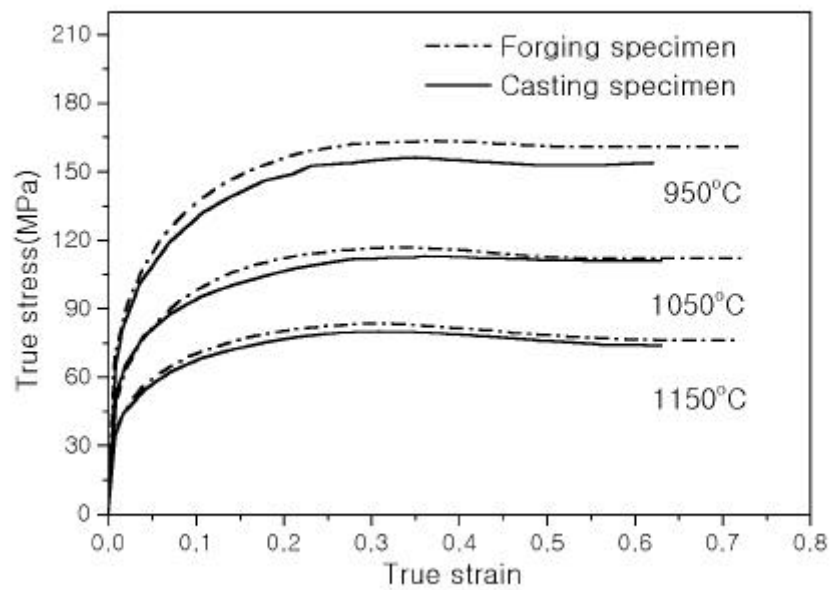


Fig. 20 Comparison of flow curves at $\dot{\epsilon}=1.0/\text{s}$

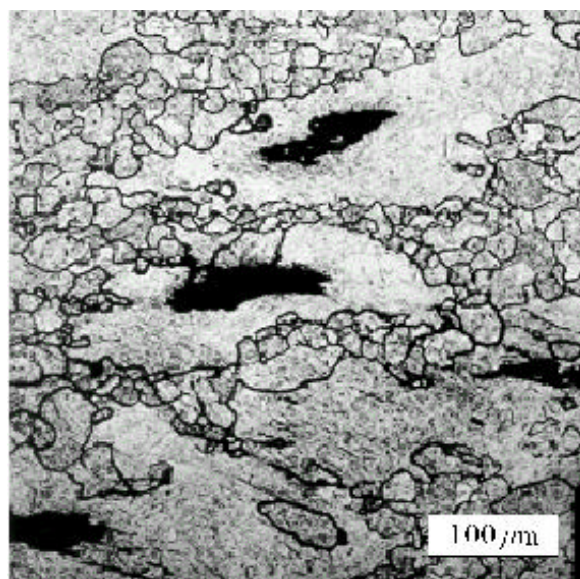


Photo 7 Microstructure of 50% compressed casting specimen at 1050°C and $\dot{\epsilon}=1.0/\text{s}$

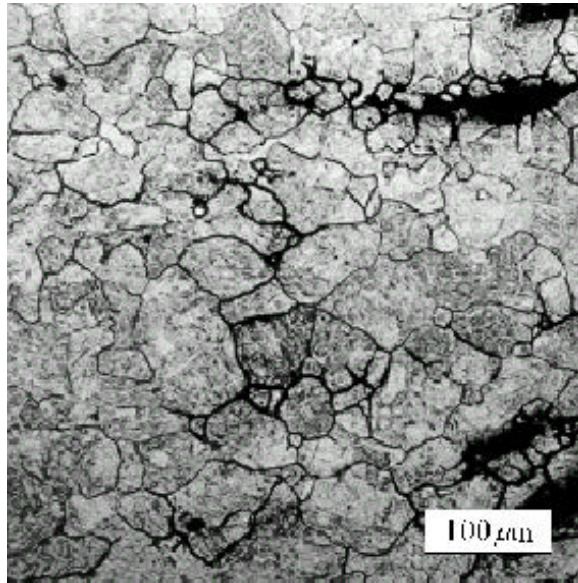


Photo 8 Microstructure of 50% compressed casting specimen at 1150 °C and $\dot{\epsilon}=1.0/\text{s}$

4.2.2

3.1.2

.

, ,

. ,

, , ,

Photo 9 16

.

5

, 가 가

, 가

. ,

가

.

Photo 9 12

950 °C ,

$\dot{\epsilon}=1.0/\text{s}$,

20%

. 950 1150
 . Photo 13 16 1150 , $\dot{\epsilon}$
 $=1.0/s$, 20% . 950
 [4] C-Mn Sellars
 950 100 , 1150 5
 가 ,
 ,
 가 .

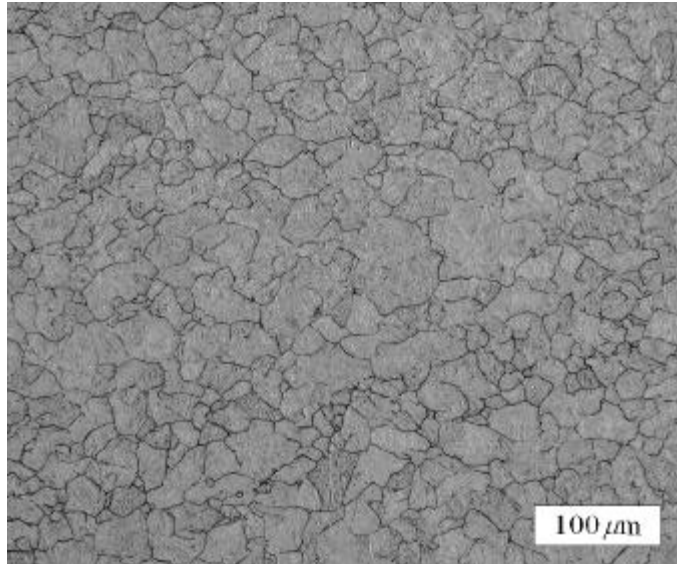


Photo 9 Microstructure of 20% compressed specimen at 950 , $\dot{\epsilon}=1.0/s$ and
 5sec holding

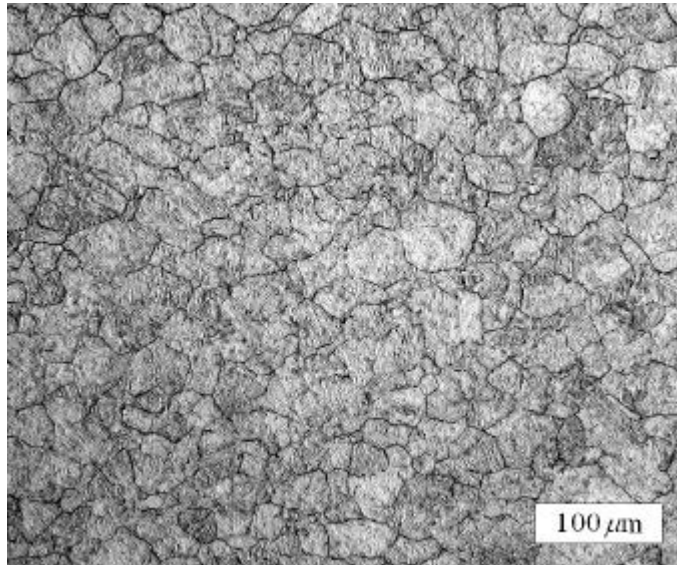


Photo 10 Microstructure of 20% compressed specimen at 950 °C, $\dot{\epsilon}=1.0/\text{s}$ and 10sec holding

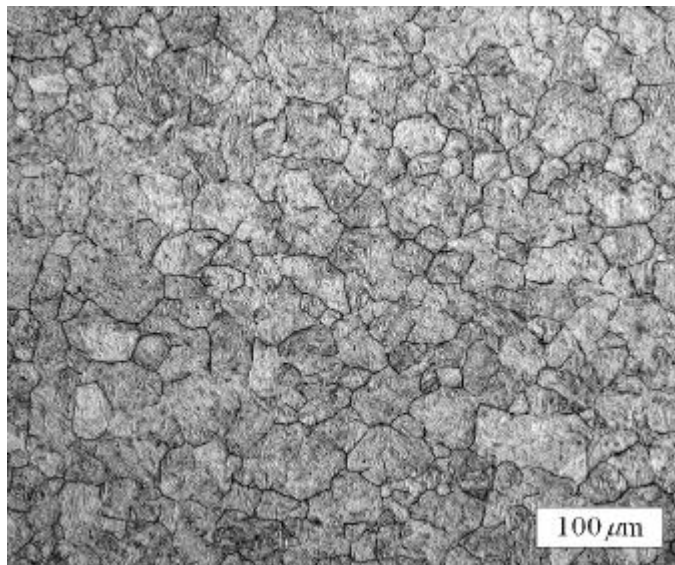


Photo 11 Microstructure of 20% compressed specimen at 950 °C, $\dot{\epsilon}=1.0/\text{s}$ and 100sec holding

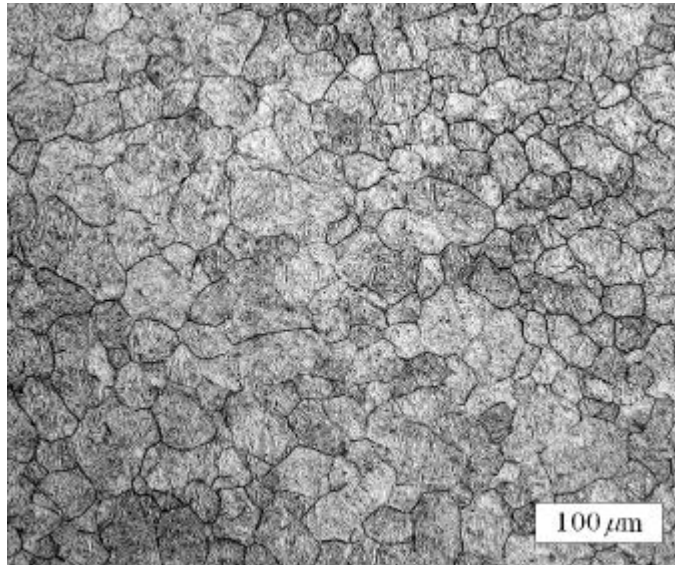


Photo 12 Microstructure of 20% compressed specimen at 950 °C, $\dot{\epsilon}=1.0/\text{s}$ and 600sec holding

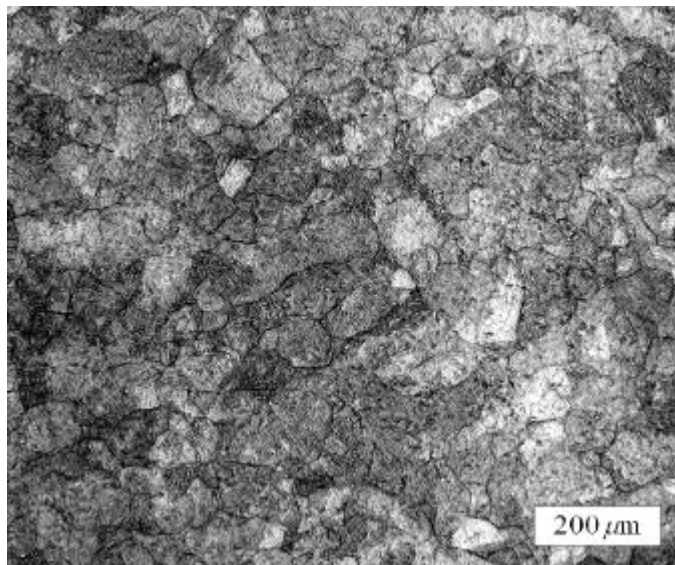


Photo 13 Microstructure of 20% compressed specimen at 1150 °C, $\dot{\epsilon}=1.0/\text{s}$ and 5sec holding

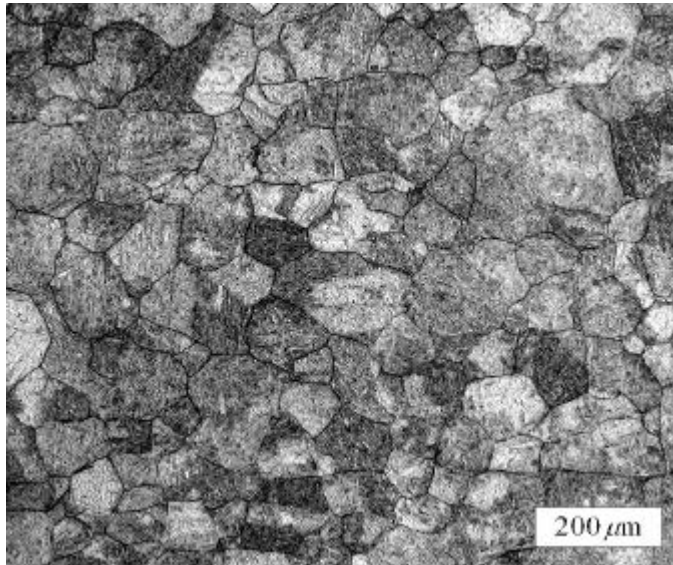


Photo 14 Microstructure of 20% compressed specimen at 1150 °C, $\dot{\epsilon}=1.0/\text{s}$ and 20sec holding

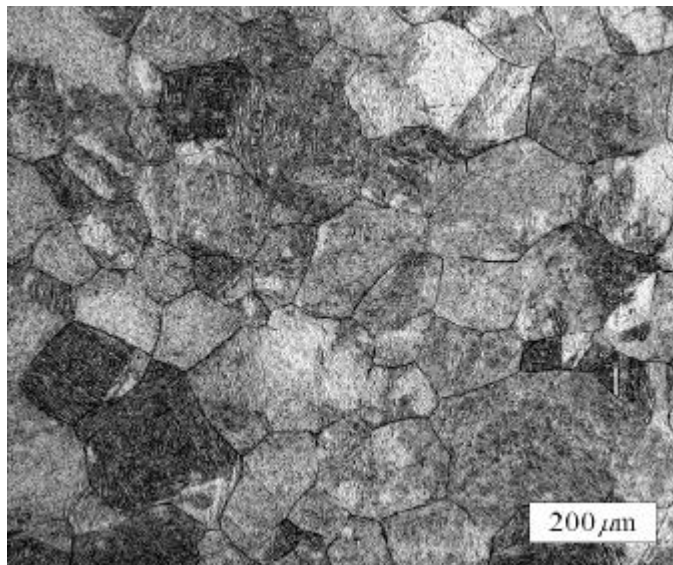


Photo 15 Microstructure of 20% compressed specimen at 1150 °C, $\dot{\epsilon}=1.0/\text{s}$ and 100sec holding

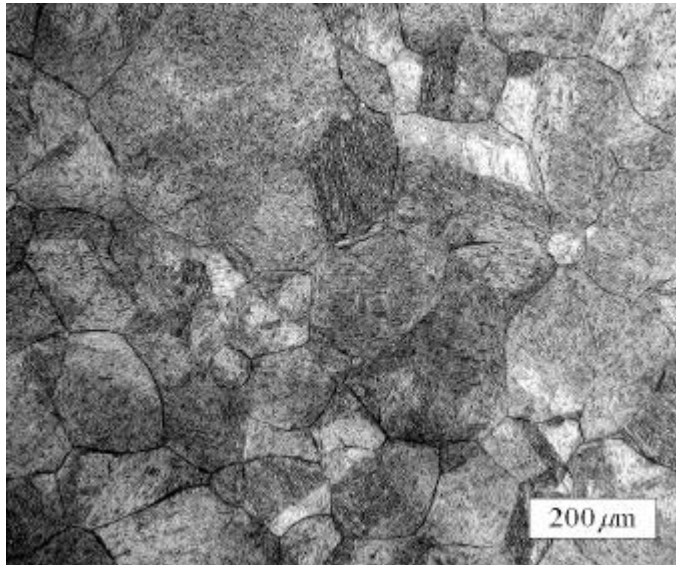


Photo 16 Microstructure of 20% compressed specimen at 1150 °C, $\dot{\epsilon}=1.0/\text{s}$ and 600sec holding

4.2.3

3.1.3 , 2

, , ,

.

Fig. 21 25 2 . Fig.

21- (a) $0.71 \epsilon_p$ 2

가 Fig. 21- (b)

$1.24 \epsilon_p$ 2

가 .

가 가

. Fig. 22- (a),(b) 950 $0.43 \epsilon_p$,

$0.82 \epsilon_p$ 2 100

가 .

Fig. 23- (a),(b) 1150 $2 \varepsilon_p, \varepsilon_p$

2 가

가

가 Fig. 24- (a),(b) 1150

$0.53 \varepsilon_p, \varepsilon_p$ $0.53 \varepsilon_p$

2 5 가

ε_p 2 가

Fig. 25- (a),(b) 2

950 100 가

1150 가 가

Fig. 26 27

Fig. 26- (a)

가 Fig. 26- (b) 가

가 가 가

Fig. 27- (a),(b) 115

0 가

Fig. 28- (a), (b) 1150

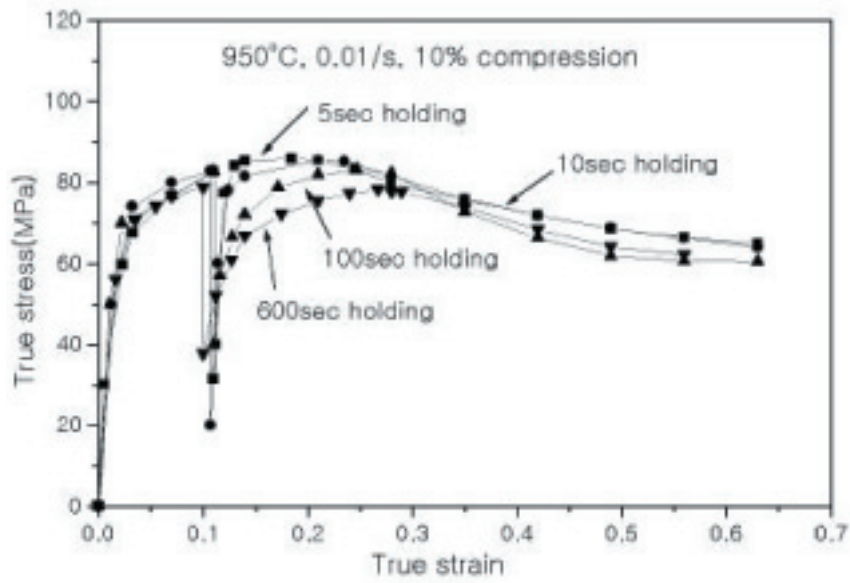
ε_p 가 0.1/ s 가 0.01/ s

Fig. 29- (a),(b)

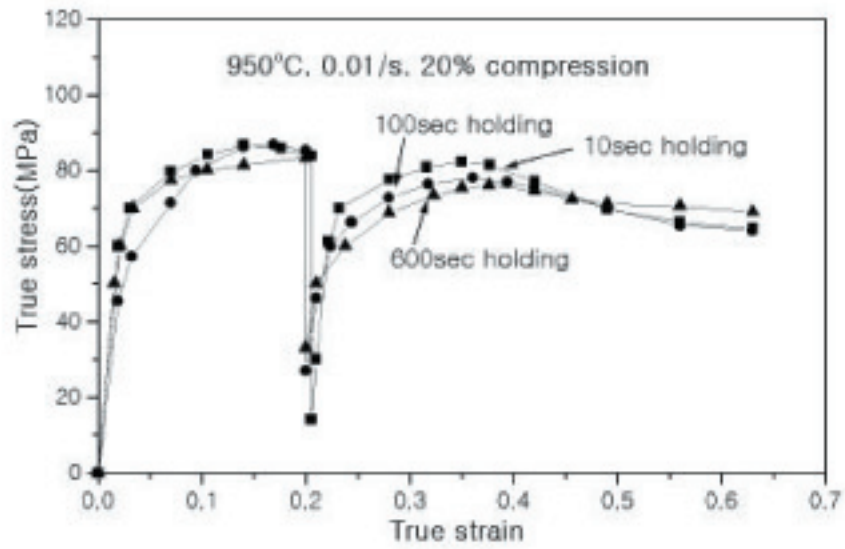
(Fig. 26 27), 가

(Fig. 28).

가 가

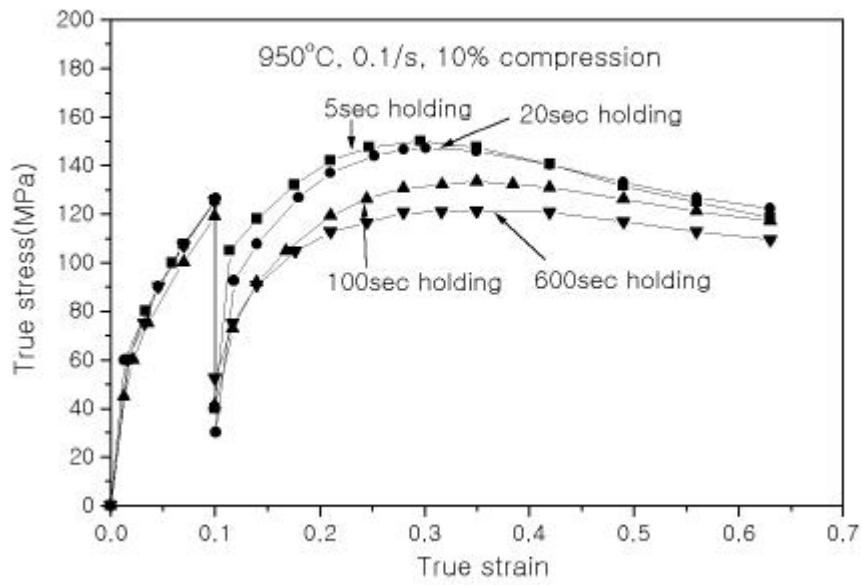


(a)

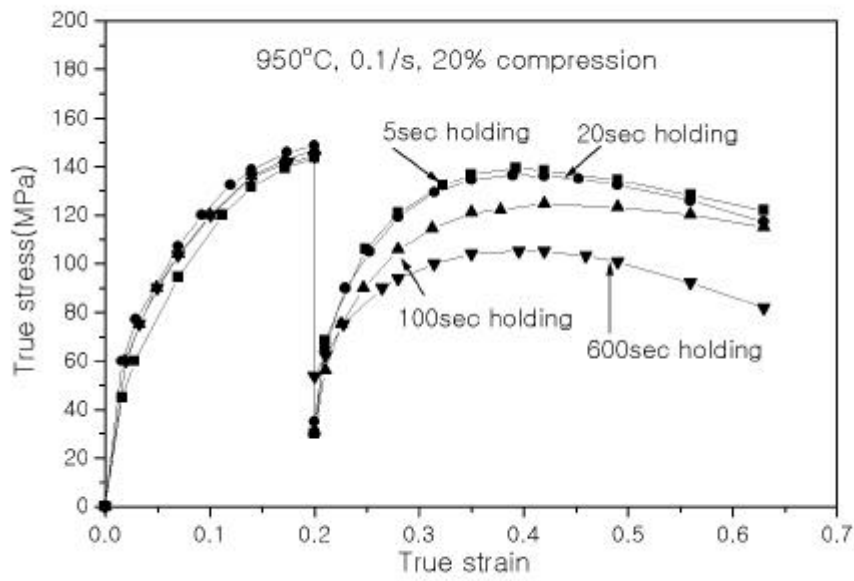


(b)

Fig. 21 Flow curves obtained from interrupted compression test at $\dot{\epsilon}=0.01/s$, 950 °C and (a) 10% compression (b) 20% compression

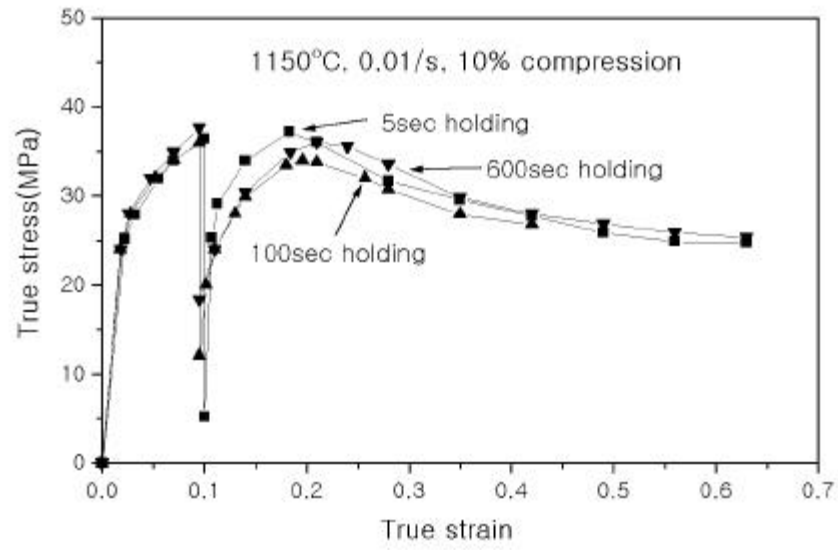


(a)

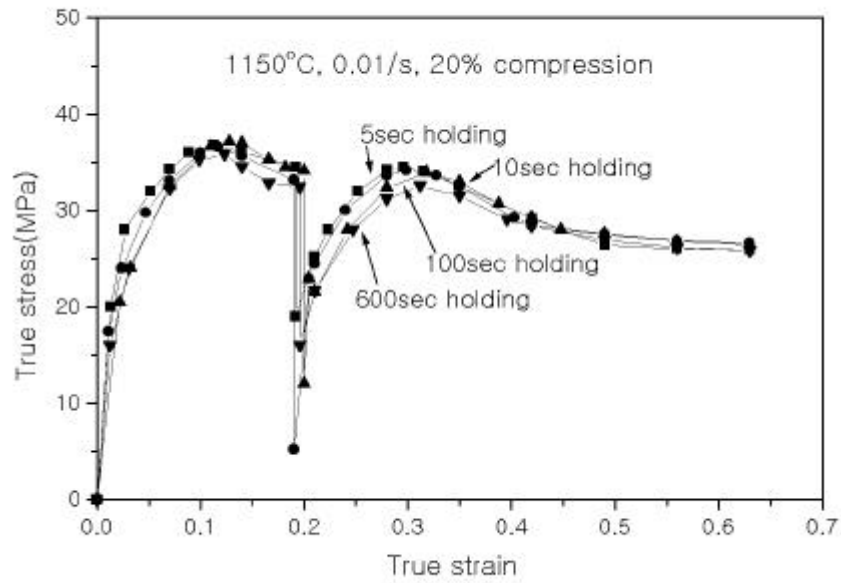


(b)

Fig. 22 Flow curves obtained from interrupted compression test at $\dot{\epsilon}=0.1/s$,
950 and (a) 10% compression (b) 20% compression

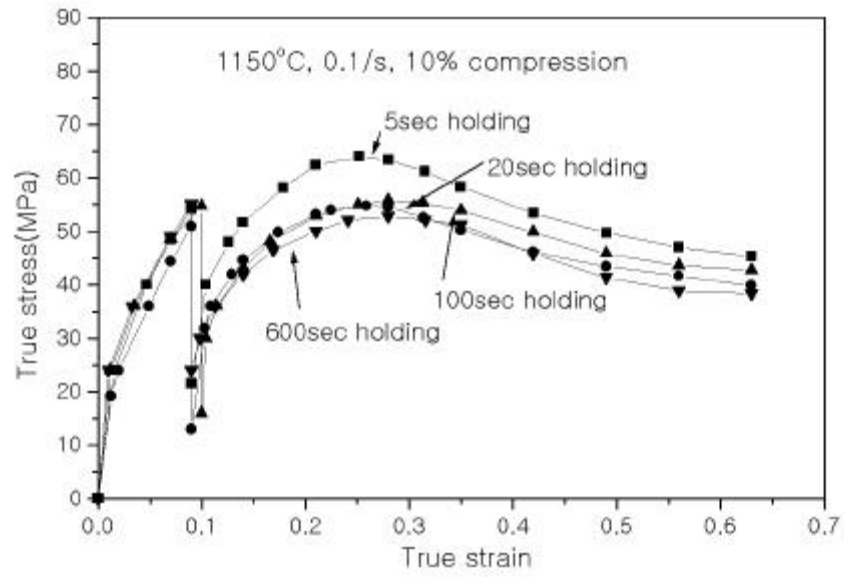


(a)

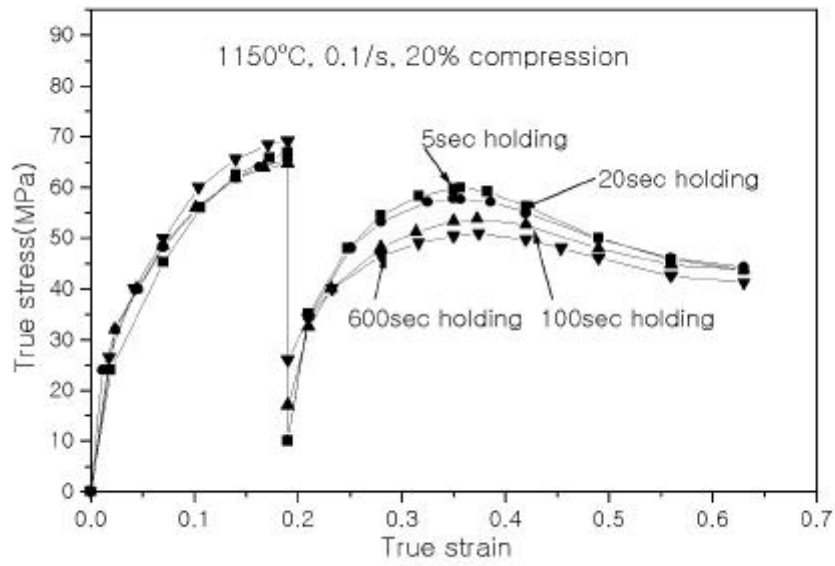


(b)

Fig. 23 Flow curves obtained from interrupted compression test at $\dot{\epsilon}=0.01/s$, 1150 and (a) 10% compression (b) 20% compression

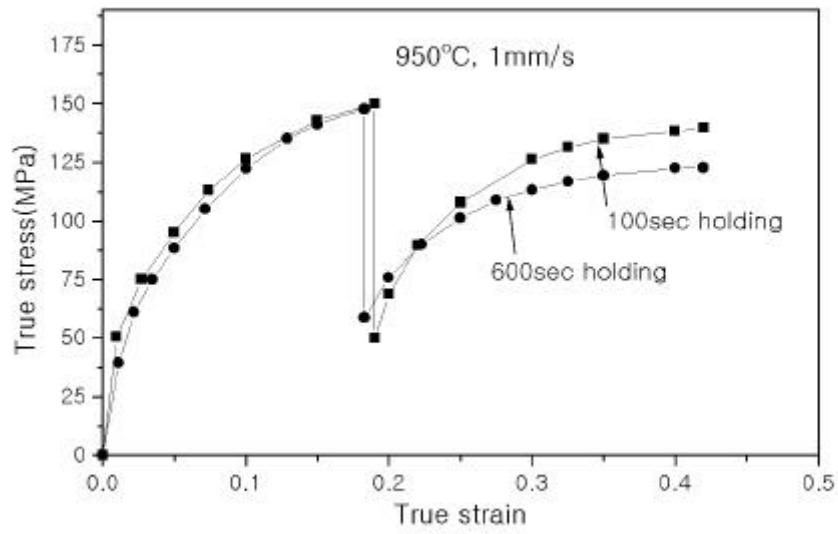


(a)

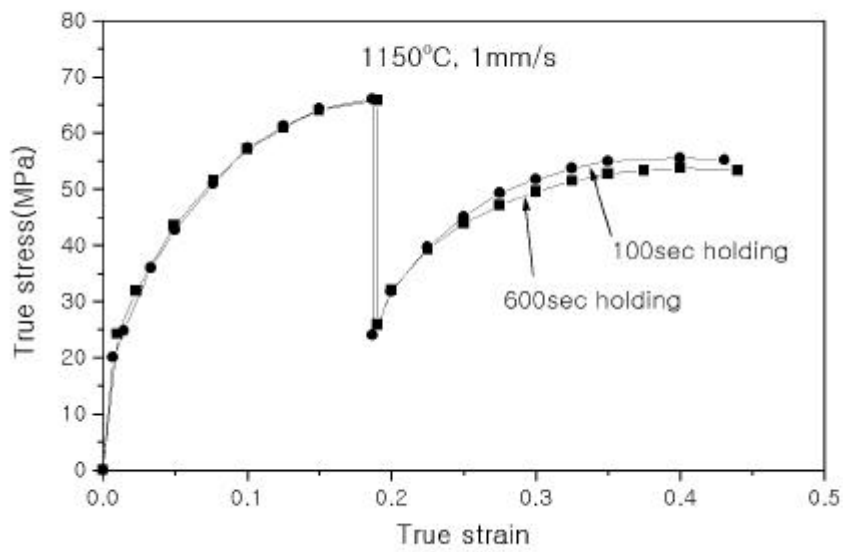


(b)

Fig. 24 Flow curves obtained from interrupted compression test at $\dot{\epsilon}=0.1/s$, 1150 and (a) 10% compression (b) 20% compression

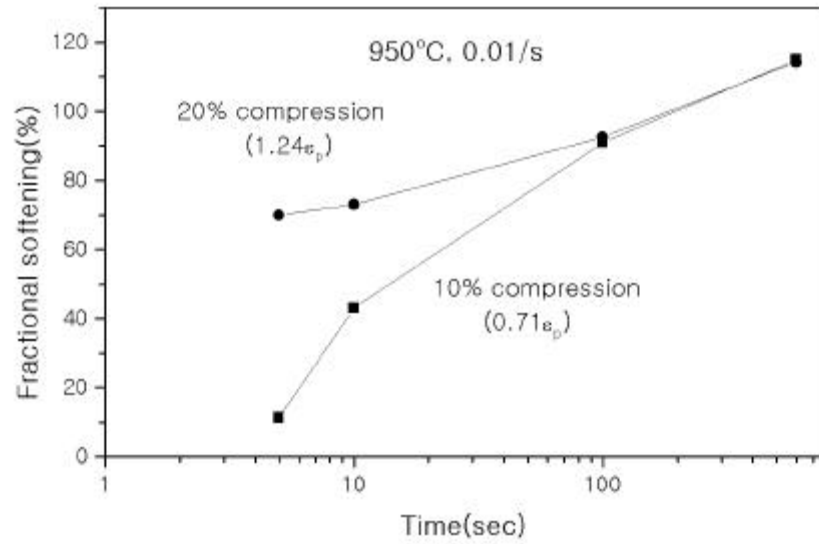


(a)

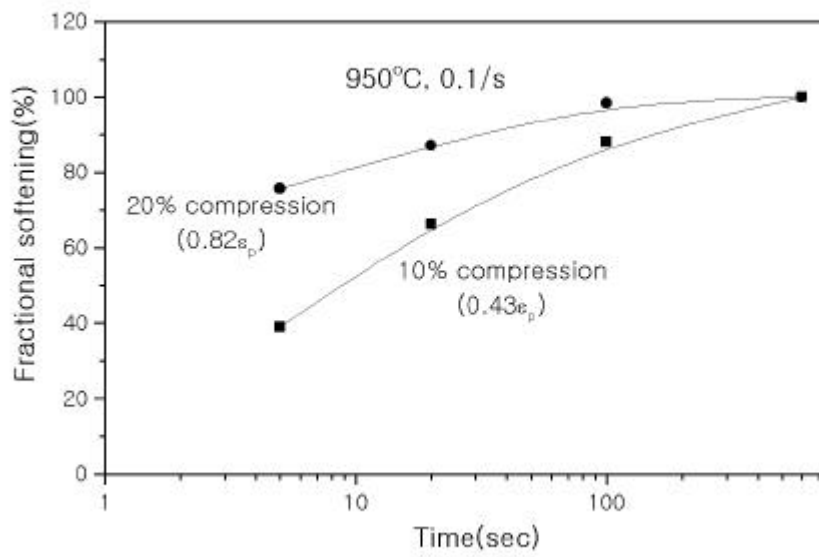


(b)

Fig. 25 Flow curves obtained from interrupted compression test at $v=1\text{mm/s}$ and (a) 950 (b) 1150

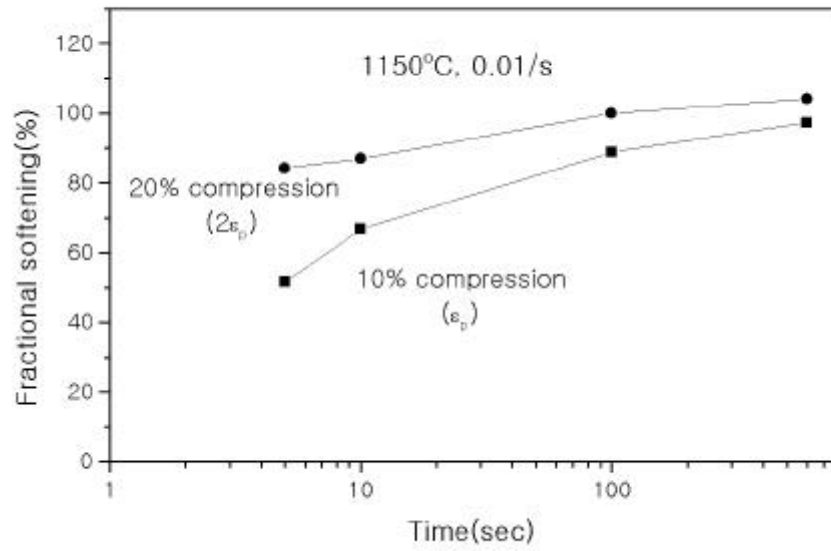


(a)

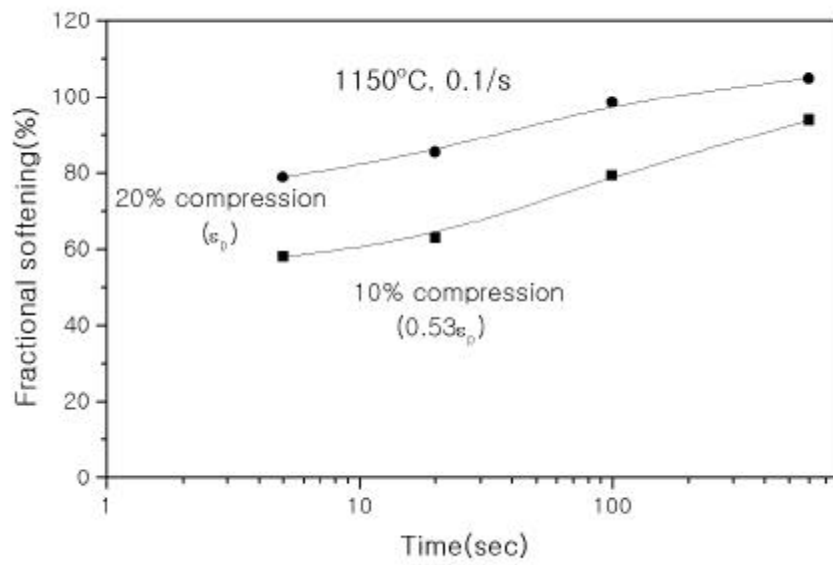


(b)

Fig. 26 Strain effect on the rate of softening at 950 °C and (a) $\dot{\epsilon}=0.01/s$
(b) $\dot{\epsilon}=0.1/s$

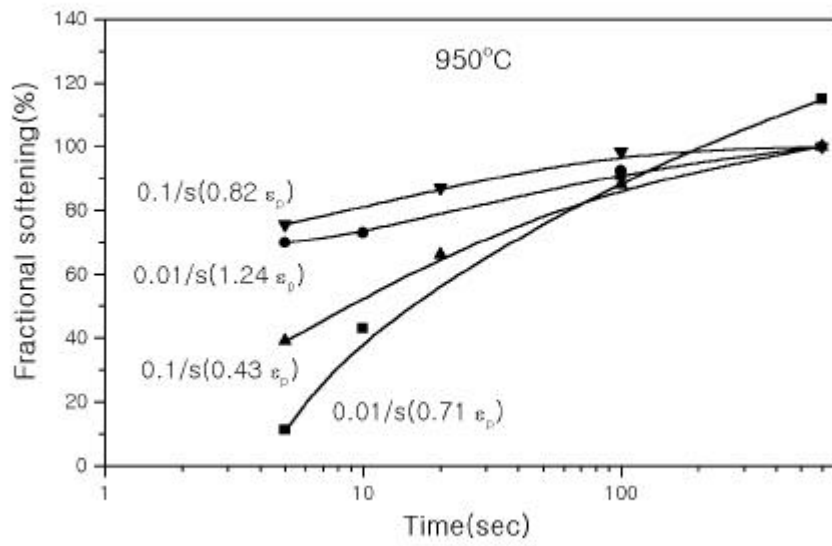


(a)

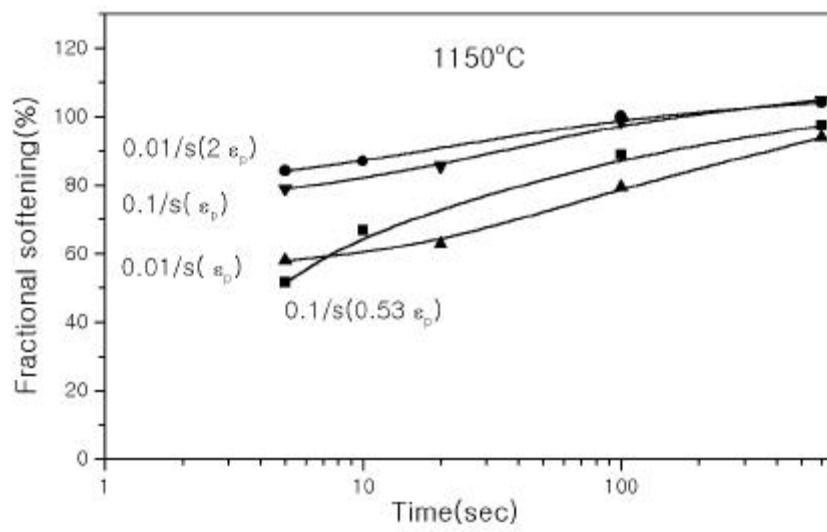


(b)

Fig. 27 Strain effect on the rate of softening at 1150 °C and (a) $\dot{\epsilon}=0.01/s$
(b) $\dot{\epsilon}=0.1/s$

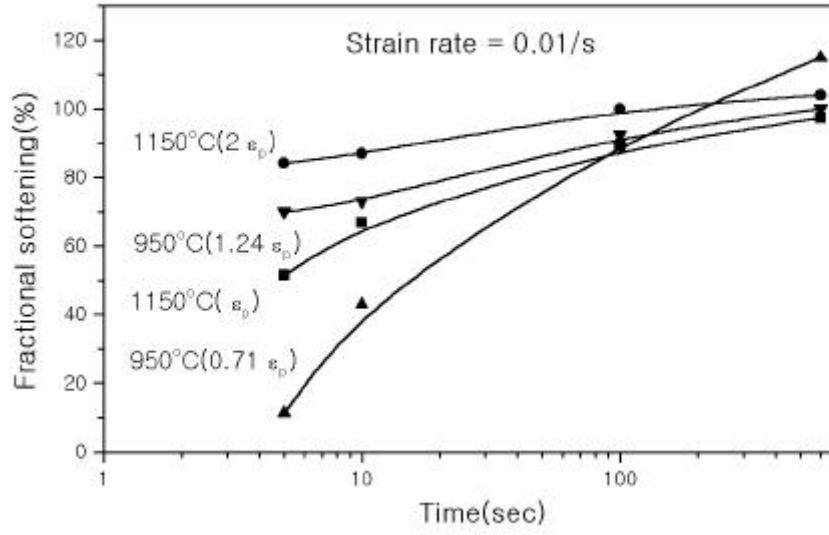


(a)

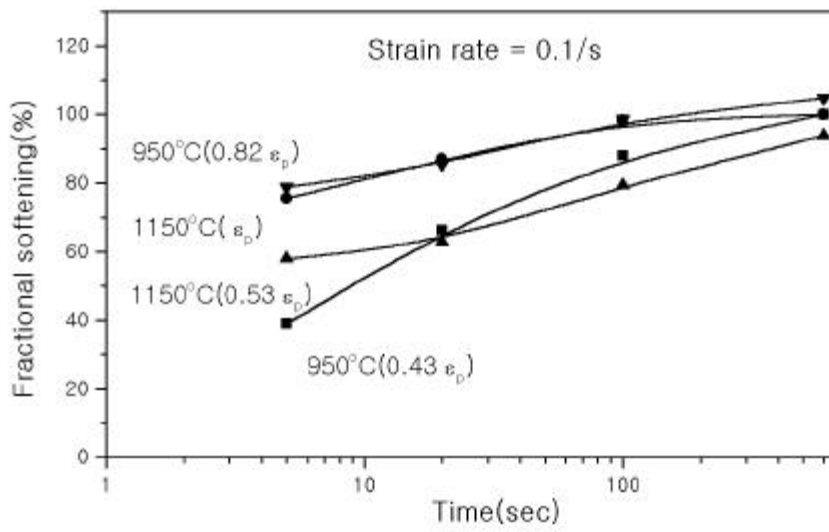


(b)

Fig. 28 Strain rate effect on the rate of softening at (a) 950 (b) 1150



(a)



(b)

Fig. 29 Temperature effect on the rate of softening at (a) $\dot{\epsilon}=0.01/s$ (b) $\dot{\epsilon}=0.1/s$

4.3

Fig.5 2

2 1mm/s, 1150 16.7%

20% 3

100sec 600sec 2

Photo 17 Photo 18 . Fig.

30 (Photo 17 18)

Photo 17 18 (1)

600 가

가 . Photo 17 18 (3)

가 Photo 17 18

(6)

Fig. 31 . Fig. 32

Fig. 33

37

. Fig. 38

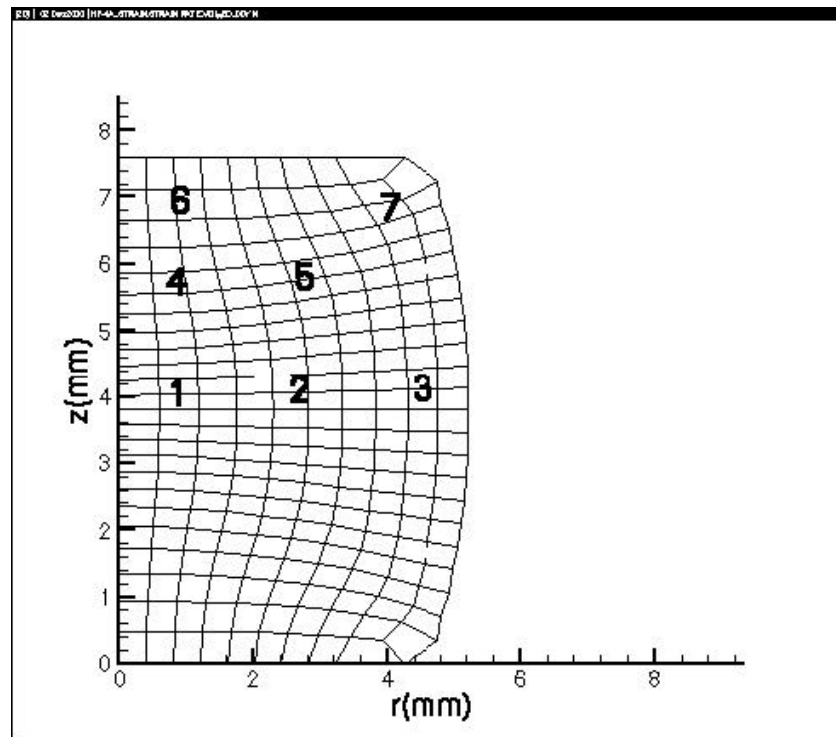
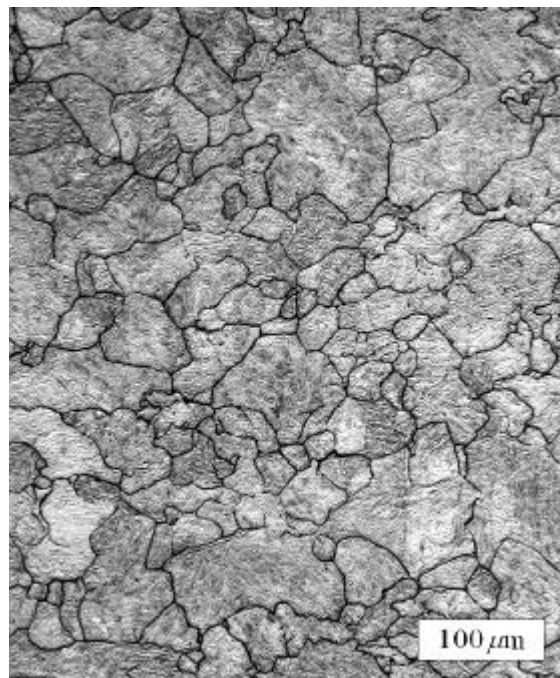
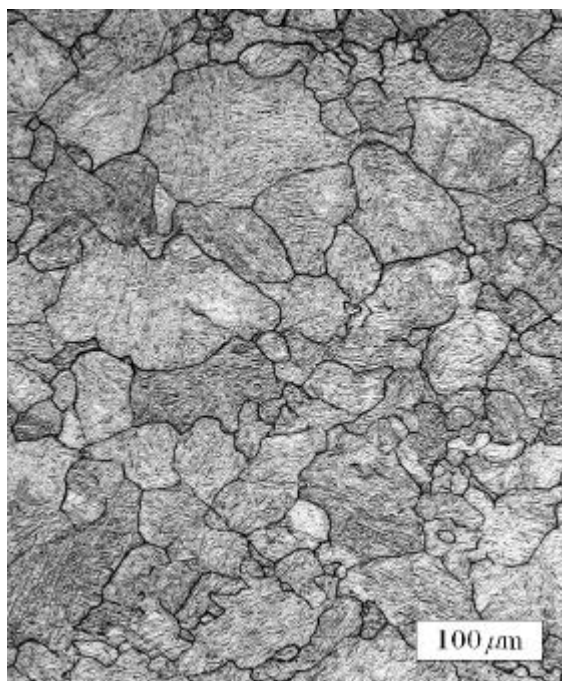


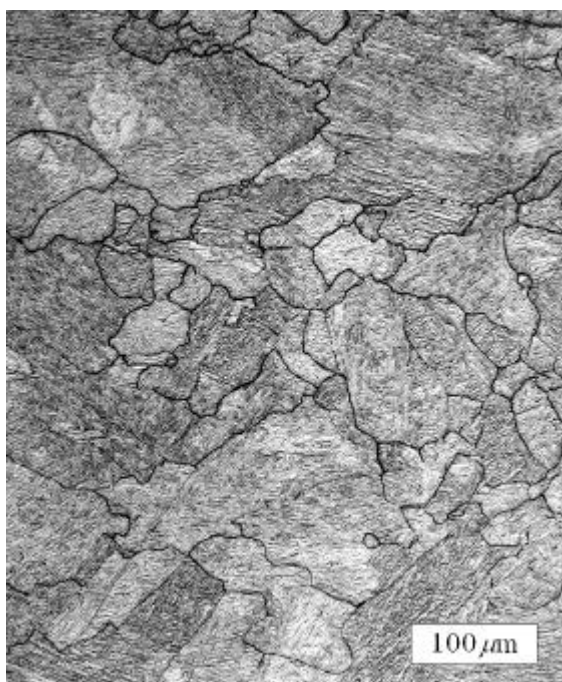
Fig. 30 Diagram for each microstructure photographic point



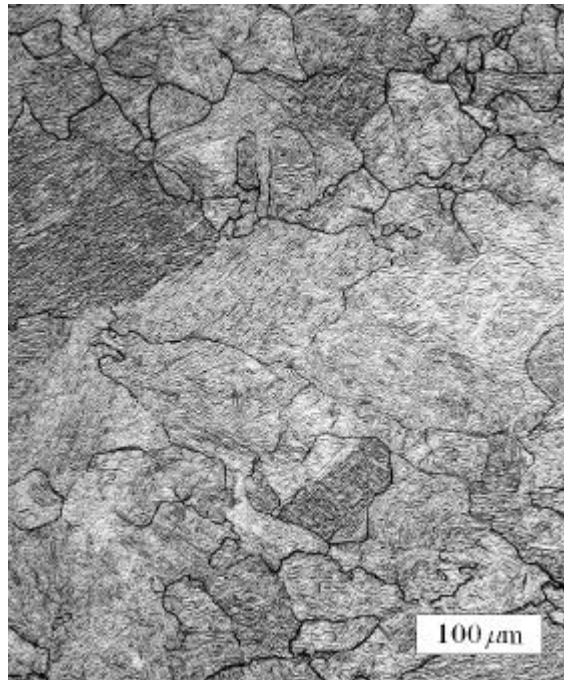
point 1



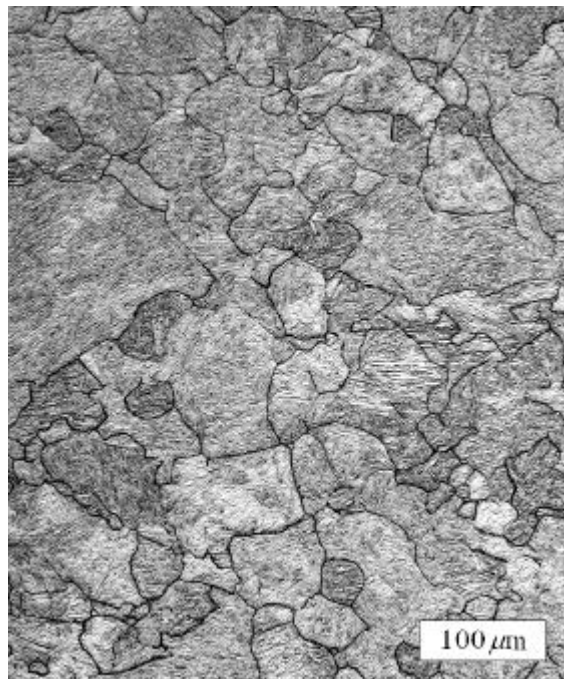
point 2



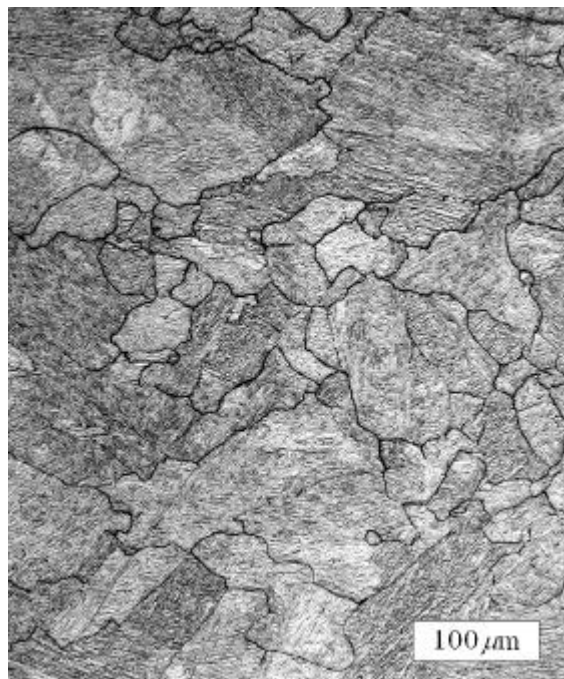
point 3



point 4

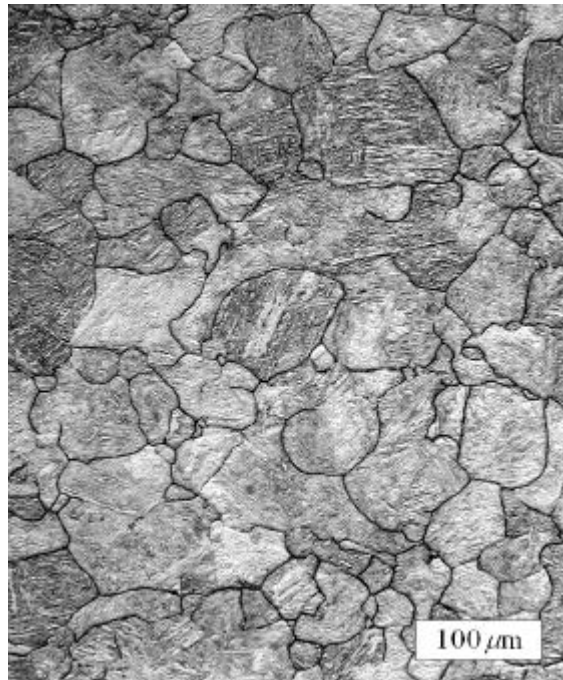


point 5

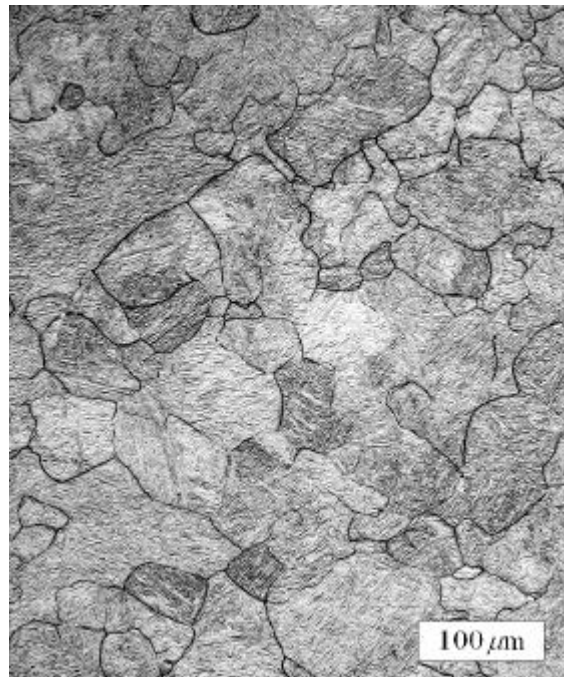


point 7

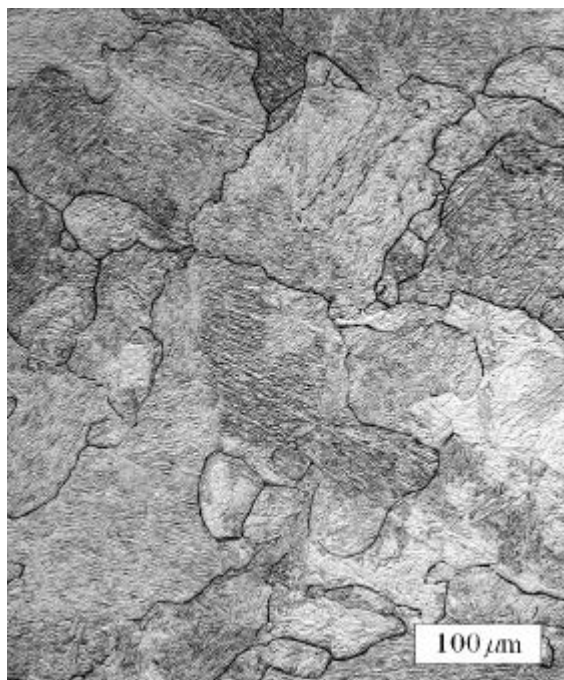
Photo 17 Microstructure of the second compression at $v=1\text{mm/s}$, 1150 and 100s holding



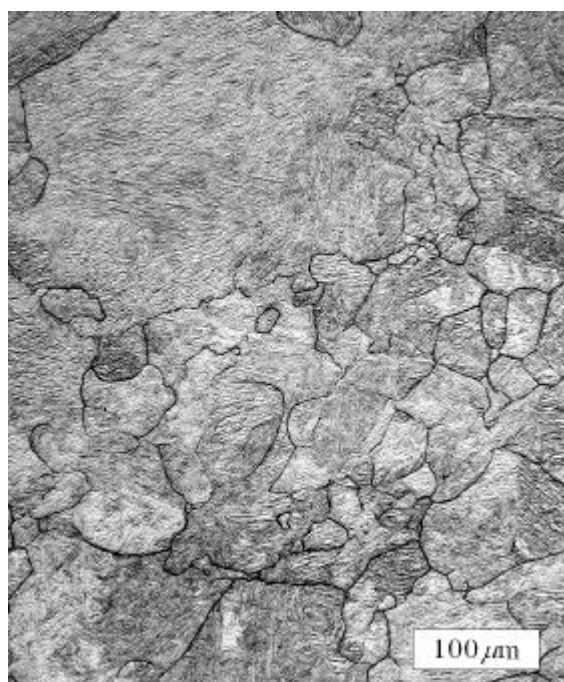
point 1



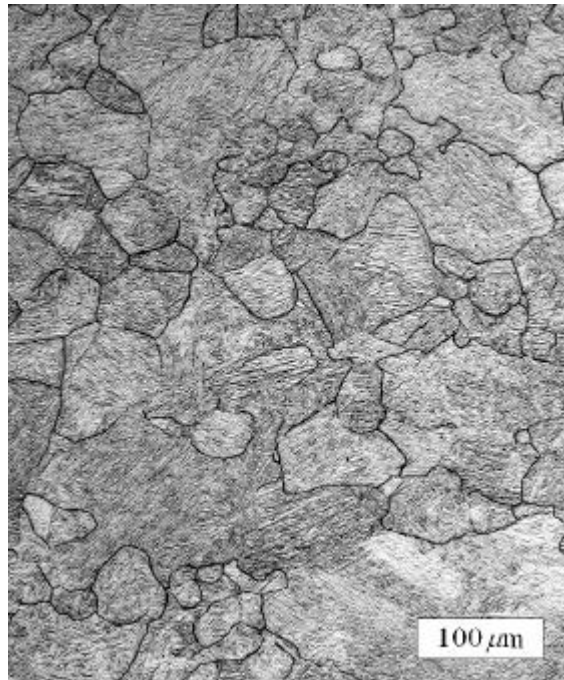
point 2



point 3



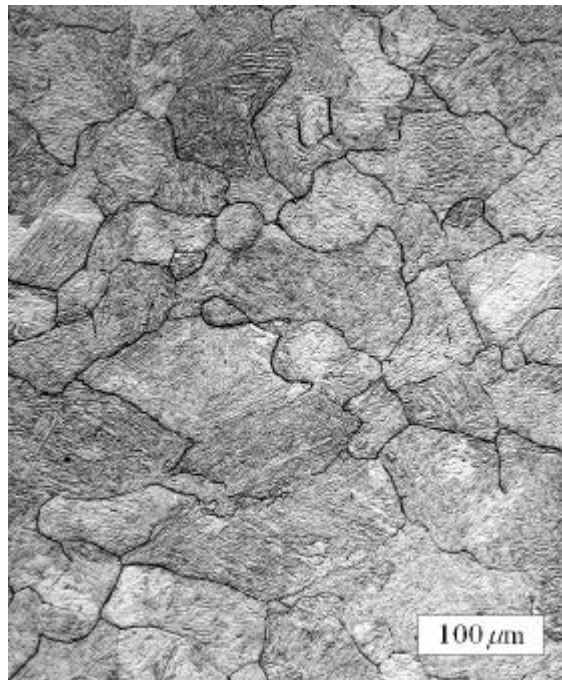
point 4



point 5

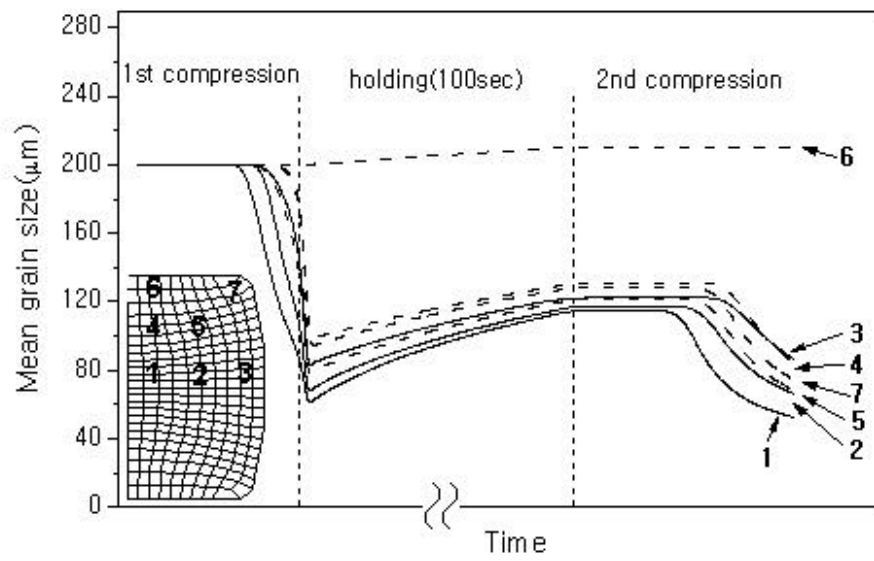


point 6

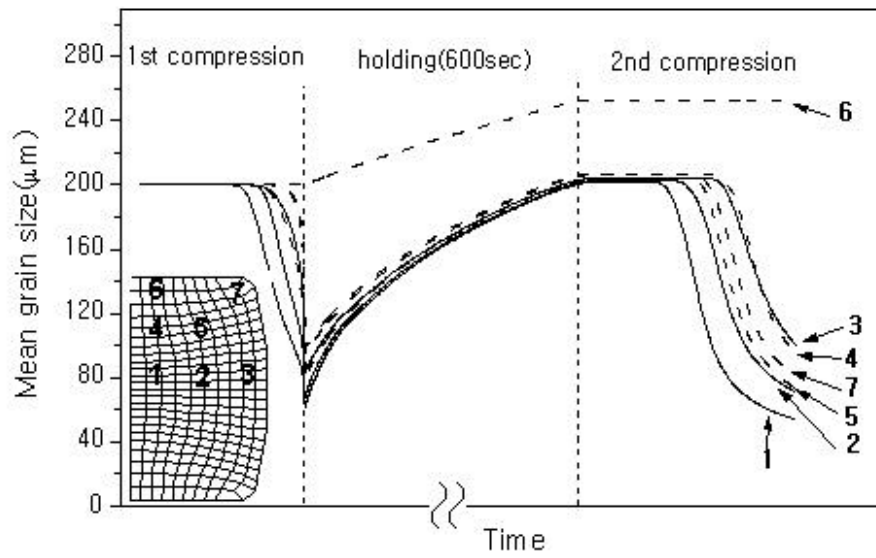


point 7

Photo 18 Microstructure of the second compression at $v=1\text{mm/s}$, 1150 and 600s holding

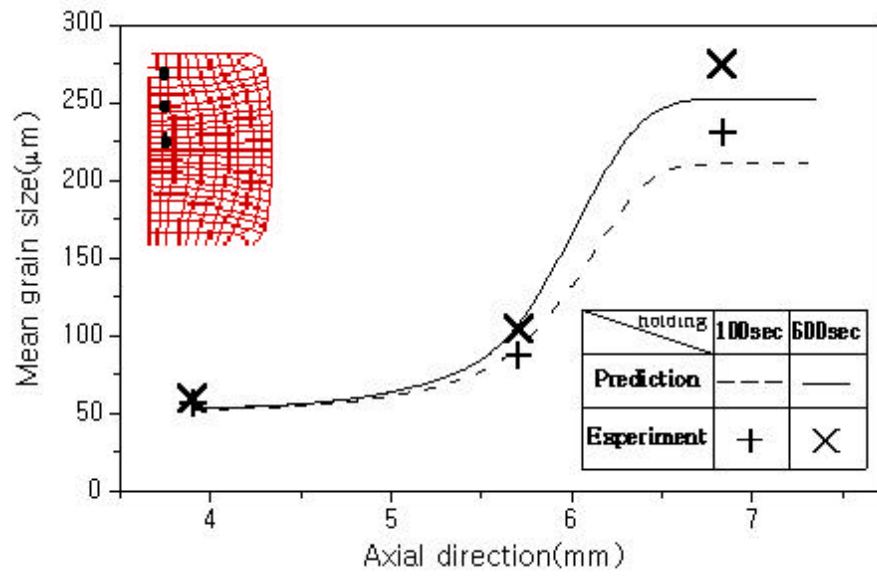


(a)

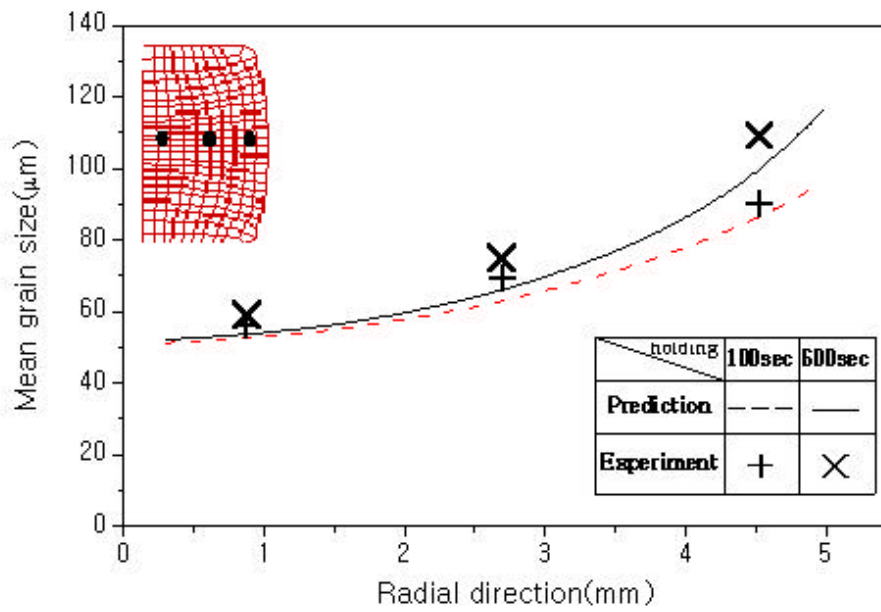


(b)

Fig. 31 Mean grain size from simulation result at $v=1\text{mm/s}$, 1150 and
(a) 100sec holding (b) 600sec holding



(a)



(b)

Fig. 32 Comparison of grain size between experimental and predicted results at $v=1\text{mm/s}$, 1150 and (a) axial direction (b) radial direction

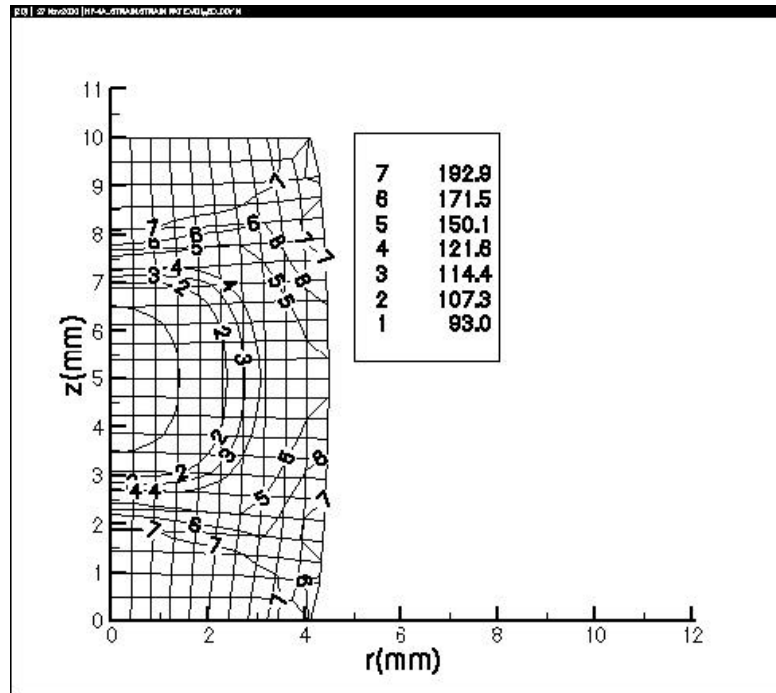


Fig. 33 Distribution of mean grain size after 16.7% second compression at $v=1\text{mm/s}$, 1150

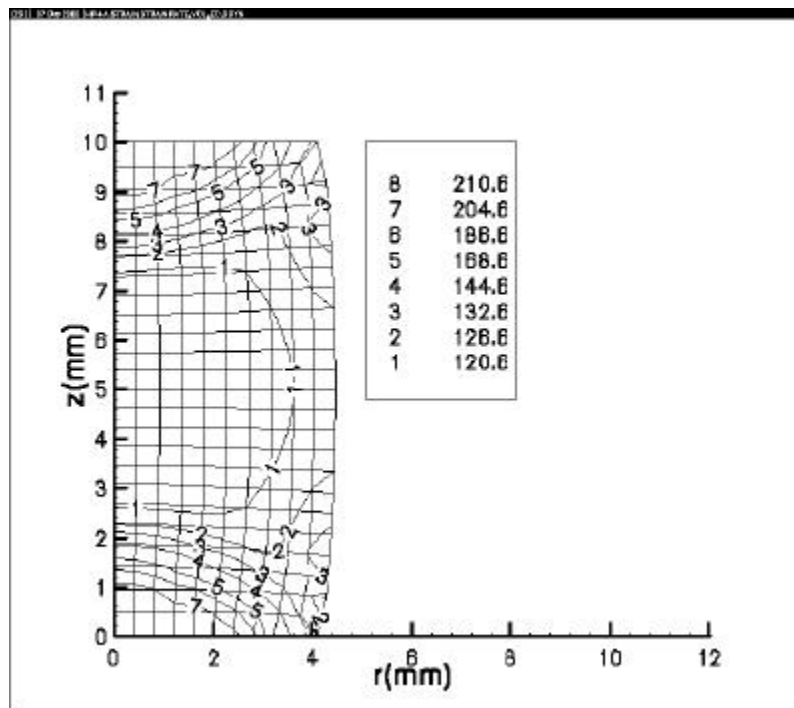


Fig. 34 Distribution of mean grain size after 100sec holding at $v=1\text{mm/s}$, 1150 and 16.7% compression

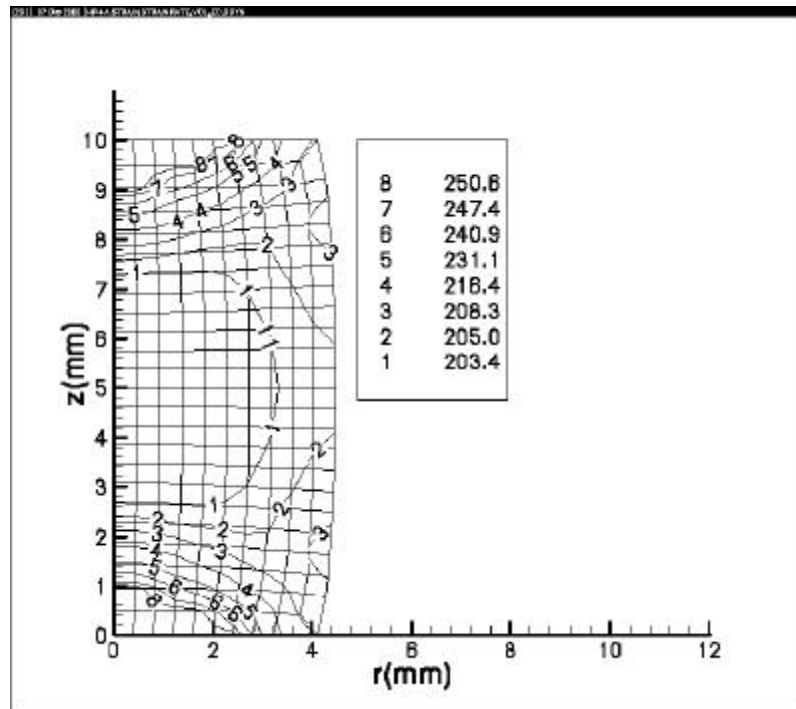


Fig. 35 Distribution of mean grain size after 600sec holding at $v=1\text{mm/s}$,
1150 °C and 16.7% compression

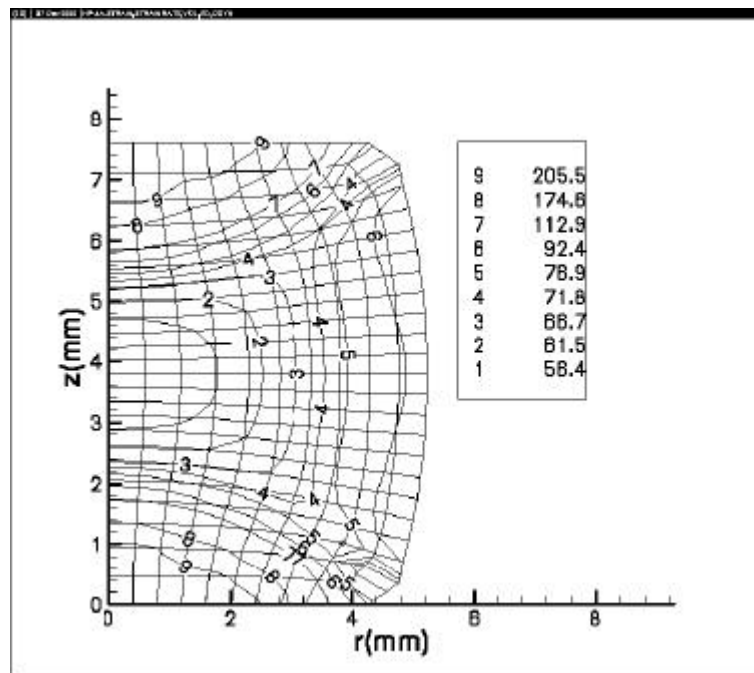


Fig. 36 Distribution of mean grain size after 36.7% second compression at
 $v=1\text{mm/s}$, 1150 °C and 100sec holding

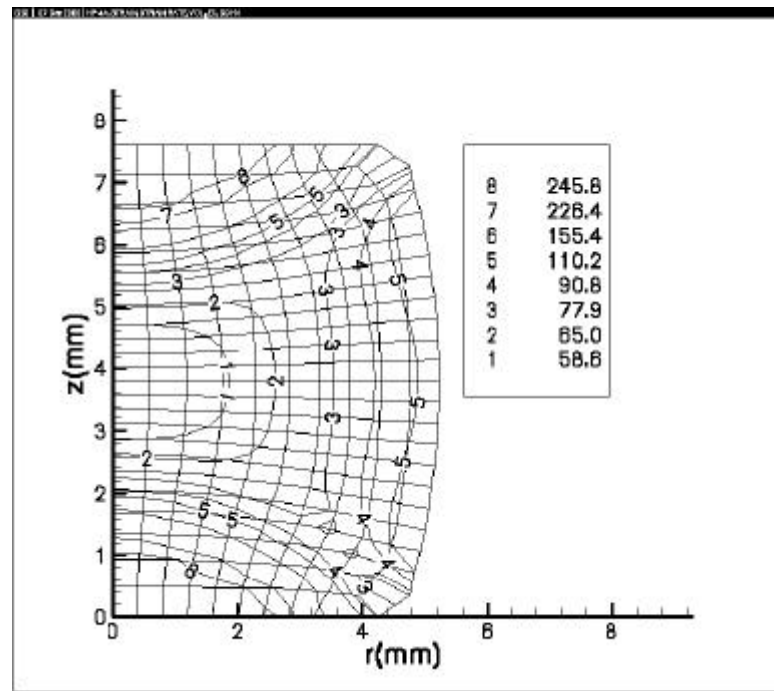


Fig. 37 Distribution of mean grain size after 36.7% second compression at $v=1\text{mm/s}$, 1150 and 600sec holding

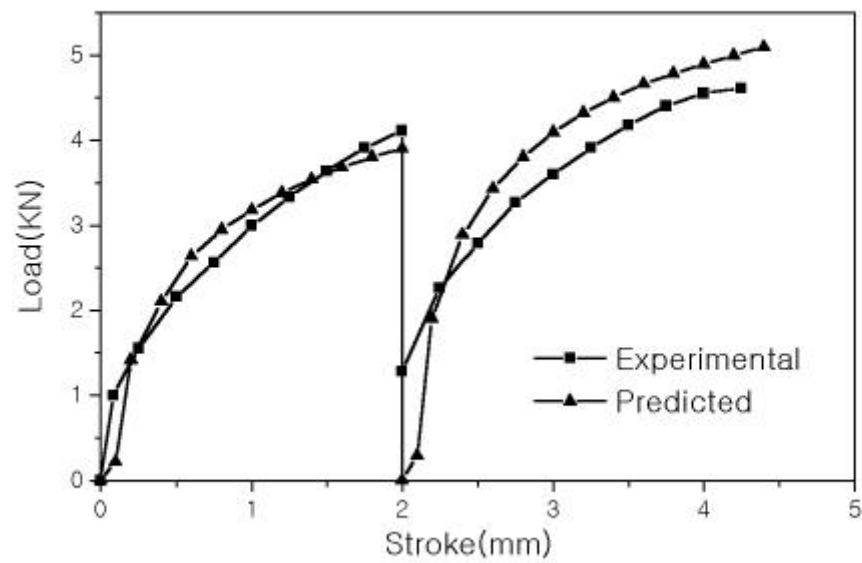


Fig. 38 Comparison of experimental and predicted load at $v=1\text{mm/s}$, 1150 and 600sec holding

5.

, .

2 ,

.

.

(1) , ,

.

$$\sigma = \sigma_p [1 - \exp(-C\varepsilon)]^m - (\sigma_p - \sigma_s) [1 - \exp(-k(\frac{\varepsilon - \alpha\varepsilon_p}{\varepsilon_p})^{m'})]$$

(2)

.

$$d_{rex} = 1.2 \cdot 10^4 Z^{-0.21}$$

$$\overline{D}^3 = D_o^3 + 1.8 \cdot 10^{16} t \exp(-\frac{Q}{R T})$$

(3)

Zener - Hollomon 가

, 가 가 가 .

(4)

Zener - Hollomon 가

, 가 가 .

(5) 2

, .

(6) , 가 , ,
가 .

(7)
,
.

- [1] C. M. Sellars, "The physical metallurgy of hot working" International Conference on Hot Working and Forming Process, University of Sheffield, pp. 3 47, 1979.
- [2] C. M. Sellars and J. A. Whiteman, "Recrystallization and grain growth in hot rolling", Metal Science, Vol. 13, pp. 187 194, 1979.
- [3] C. M. Sellars, "Modelling microstructural development during hot rolling", Materials Science and Technology, Vol. 6, pp. 1072 1081, 1990.
- [4] John H. Beynon and C. Michael Sellars, "Modelling microstructure and its effects during multipass hot rolling", ISIJ International, Vol. 32, No. 3, pp. 359 367, 1992.
- [5] S. F. Medina and C. A. Hernandez, "General expression of the Zener-Hollomon parameter as a function of the chemical composition of low alloy and microalloyed steels", Acta Mater, Vol. 44, No. 1, pp. 137 148, 1996.
- [6] S. F. Medina and C. A. Hernandez, "The influence of chemical composition on peak strain of deformed austenite in low alloy and microalloyed steels", Acta Mater, Vol. 44, No. 1, pp. 149 154, 1996.
- [7] C. A. Hernandez, S. F. Medina and J. Ruiz, "Modelling austenite flow curves in low alloy and microalloyed steels", Acta Mater, Vol. 44, No. 1, pp. 155 163, 1996.
- [8] S. F. Medina and C. A. Hernandez, "Modelling of the dynamic recrystallization of austenite in low alloy and microalloyed steels", Acta Mater, Vol. 44, No. 1, pp. 165 171, 1996.
- [9] D. G. Martin, "Computer simulation of recrystallisation and grain growth", Materials Science and Technology, Vol. 10, October 1994.

- [10] A. Laasraoui and J. J. Jonas, "Prediction of steel flow stresses at high temperatures and strain rates", Metall. Trans. A22A, 1545, 1991.
- [11] K. P. Rao and E. B. Hawbolt, "Development of constitutive relationships using compression testing of a medium carbon steel", Journal of Engineering Materials and Technology, Vol. 114, pp. 116-123, 1992.
- [12] D. Zhao, S. Tangrila, M. Thirukkonda, K. G. Anand, and K. C. Bearden "Flow behavior and critical strain for dynamic recrystallization in HY-100 Steel", 37TH MWSP CONF. PROC., ISS, Vol. XXXIII, pp. 669-679, 1996.
- [13] , , , , , "Al6061", , Vol. 36, No. 4, pp. 502-508, 1998.
- [14] J. R. Cho, W. B. Bae, W. J. Hwang, "A study of the hot deformation behaviour and dynamic recrystallization of Al-5wt%Mg alloy", accepted J. of Mat. Processing Technology, 2000.
- [15] W. P. Sun and E. B. Hawbolt, "Comparison between static and metadynamic recrystallization - An application to the hot rolling of steels", ISIJ International, Vol. 37, No. 10, pp. 1000-1009, 1997.
- [16] C. A. Dandre, S. M. Roberts, R. W. Evans and R. C. Reed, "Prediction of microstructural evolution during cogging of Inconel 718: Process Modelling and Validation", Confidential Report
- [17] , , " ", , Vol. 14, No. 9, pp. 90-100, 1997.
- [18] , , , , " ", 가 , Vol. 5, No. 4, pp. 305-319, 1996.
- [19] , , , , " Inconel 718 ", 가 , Vol. 35, No. 6, pp. 197-206, 1998.
- [20] , , , " Al-5wt%Mg ", 가 , Vol. 8, No. 6, pp. 620-625, 1999.

- [21] , , , , “SCM 440
”, , Vol. 9, No. 1, pp. 80-87,
2000.
- [22] Imao Tamura, "Some fundamental steps in thermomechanical processing of
steels", Transactions ISIJ, Vol. 27, 1987.
- [23] H. J. McQueen, "Metal forming: Industrial, mechanical computational and
microstructural", Journal of Materials Processing Technology, Vol. 37, pp.
3-36, 1993.
- [24] D. R. Barraclough, "Hot working and recrystallisation of a stainless and a
low alloy steel", Ph. D. dissertation, University of Sheffield, 1974.
- [25] , “3 - ”,
, 1993.
- [26] , “ ”, , 1998.